JCB Journal of Cell Biology

ARTICLE

Fatty acid–binding proteins 3, 7, and 8 bind cholesterol and facilitate its egress from lysosomes

Xian-Xiu Fang[1*], Pengcheng Wei[1*], Kai Zhao[1], Zhao-Chen Sheng[1], Bao-Liang Song[1], Lei Yin[1], and Jie Luo[1]

Cholesterol from low-density lipoprotein (LDL) can be transported to many organelle membranes by non-vesicular mechanisms involving sterol transfer proteins (STPs). Fatty acid–binding protein (FABP) 7 was identified in our previous study searching for new regulators of intracellular cholesterol trafficking. Whether FABP7 is a bona fide STP remains unknown. Here, we found that FABP7 deficiency resulted in the accumulation of LDL-derived cholesterol in lysosomes and reduced cholesterol levels on the plasma membrane. A crystal structure of human FABP7 protein in complex with cholesterol was resolved at 2.7 Å resolution. In vitro, FABP7 efficiently transported the cholesterol analog dehydroergosterol between the liposomes. Further, the silencing of FABP3 and 8, which belong to the same family as FABP7, caused robust cholesterol accumulation in lysosomes. These two FABP proteins could transport dehydroergosterol in vitro as well. Collectively, our results suggest that FABP3, 7, and 8 are a new class of STPs mediating cholesterol egress from lysosomes.

Introduction

Cholesterol is dynamically transported between different organelle membranes in mammalian cells for the regulation of membrane property and function, biosynthesis of steroid hormones and bile acids, and modification of the Hedgehog and Smoothened proteins (Dietschy, 2009; Luo et al., 2019; Porter et al., 1996; Xiao et al., 2017; Hu et al., 2022; Qiu et al., 2023). A way to obtain exogenous cholesterol is the receptor-mediated endocytosis of low-density lipoproteins (LDLs). Once in the cell, cholesterol is liberated from cholesteryl esters as LDL is sorted along the endocytic pathway to lysosomes, where cholesterol is then inserted into the lysosomal membrane by the coordinated actions of Niemann-Pick C (NPC) 1 and NPC2 proteins (Brown and Goldstein, 1986; Kwon et al., 2009), as well as lysosomal-associated membrane protein (LAMP) 2 and lysosomal integral membrane protein 2 (Heybrock et al., 2019; Li and Pfeffer, 2016). From lysosomes, cholesterol continues its journey to several destinations, including the plasma membrane (PM), endoplasmic reticulum (ER), and peroxisome, for structural and functional needs (Chu et al., 2015; Luo et al., 2017, 2019; Xiao et al., 2019).

Sterol transfer proteins (STPs) are critically involved in non-vesicular cholesterol transport within the cell. By virtue of an internal hydrophobic cavity, STPs shield cholesterol inside and facilitate its transport over long distances or between two closely apposed membranes (Wong et al., 2019). Many STPs can be grouped into three families: the oxysterol-binding protein (OSBP)-related protein (ORP) family, the steroidogenic acute regulatory protein-related lipid transfer domain (STARD) family, and the GRAM domain-containing protein (GRAMD) family (Luo et al., 2019). The STPs responsible for cholesterol egress from lysosomes include ORP1 (Dong et al., 2019; Zhao and Ridgway, 2017; Zhao et al., 2020), ORP5 (Du et al., 2011), STARD3 (Charman et al., 2010), and GRAMD1B (Höglinger et al., 2019). The importance of lysosomal cholesterol exit is highlighted by the NPC disease, which is caused by *NPC1* or *NPC2* mutations and characterized by cholesterol sequestration within the lysosomes of many tissues, particularly the liver, spleen, and brain (Vanier, 2010). Lysosomal cholesterol accumulation is also found in neurodegenerative diseases and peroxisomal disorders (Nixon, 2004; Malnar et al., 2014; Chu et al., 2015; Xiao et al., 2021a). Given such a pivotal role of lysosomes in cholesterol trafficking, it is tempting to speculate that there are additional STPs mediating post-lysosomal cholesterol transport.

Brain fatty acid–binding protein (a.k.a. FABP7) was one of the 341 genes highly enriched in our previous study to identify new regulators of intracellular cholesterol trafficking (Chu et al., 2015). As suggested by the name, FABP7 is abundant in the brain cells, particularly the nucleus and cytoplasm of neural

[1]The Institute for Advanced Studies, College of Life Sciences, Hubei Key Laboratory of Cell Homeostasis, Taikang Center for Life and Medical Sciences, Taikang Medical School, Frontier Science Center for Immunology and Metabolism, Wuhan University, Wuhan, China.

*X.-X. Fang and P. Wei contributed equally to this paper. Correspondence to Bao-Liang Song: blsong@whu.edu.cn; Lei Yin: yinlei@whu.edu.cn; Jie Luo: jieluo@whu.edu.cn.

progenitor cells and astrocytes, with important roles in glial differentiation and proliferation, malignant glioma migration, and neurogenesis (Driessen et al., 2018; Ebrahimi et al., 2016; Mita et al., 2010; Wolfrum, 2007). FABP7 deficiency or mutation has been closely implicated in mental health disorders including schizophrenia, autism, and bipolar disorder (Ayalew et al., 2012; Iwayama et al., 2010; Ziats and Rennert, 2011). FABP7 has a high affinity for n-3 and n-9 polyunsaturated fatty acids and is able to facilitate the transportation of docosahexaenoic acid, eicosapentaenoic acid, and oleic acid (Balendiran et al., 2000). However, it is unclear whether FABP7 is able to bind and mobilize cholesterol.

In this study, we show that FABP7 depletion leads to cholesterol accumulation in lysosomes and reduced cholesterol transport to the PM. The crystal structure analyses reveal the presence of a cholesterol molecule in human FABP7 protein. Using the in vitro transport assay, we show that FABP7 directly transports dehydroergosterol (DHE) between the liposomes. In addition to FABP7, FABP3 and FABP8 can bind and transfer cholesterol, and deficiency of FABP3 or FABP8 results in lysosomal cholesterol accumulation as well. Taken together, our work reveals a new role of FABP3, 7, and 8 in intracellular cholesterol trafficking.

Results

FABP7 deficiency results in cholesterol accumulation in lysosomes

FABP7 is reported to be a cytosolic protein capable of extracting, delivering, or exchanging fatty acids to regulate cell proliferation (Elsherbiny et al., 2013). Indeed, FABP7 showed a diffuse cytoplasmic pattern in the cells immediately fixed for immunostaining (top row, Fig. S1 A). However, by using digitonin to breach the PM and release the cytosolic components prior to fixation as previously described (Khan et al., 2013), we observed a punctate staining of FABP7 (bottom row, Fig. S1 A). Further examination using various organelle markers revealed a partial colocalization between FABP7 and the lysosomal marker LAMP1 (Fig. S1, B and C).

To test whether FABP7 is involved in cholesterol egress from lysosomes, we knocked down FABP7 using three individual siRNAs (Fig. S1, D and E) and detected robust filipin staining in lysosomes of SV589 cells (Fig. 1, A and B) and human glioma U251 cells (Fig. 1, C and D). To confirm whether the loss of FABP7 causes cholesterol accumulation in lysosomes, we generated two lines of *FABP7* knockout (KO) cells using the guide RNAs targeting the exon 2 of the FABP7 gene (Fig. S1, F and G). Consistent with the knockdown results, the knockout of FABP7 resulted in intense filipin staining within apparently enlarged lysosomes (Fig. 1, E and F). We further measured lysosomal cholesterol levels using biochemical methods. Lysosomes were isolated using iodixanol gradient centrifugation as previously described (Chu et al., 2015; Xiao et al., 2019), and the purity was verified by immunoblotting with various organelle markers (Fig. S1 H). Cholesterol was then extracted from the purified lysosomes and quantified with the Amplex Red Cholesterol Assay Kit. The results showed, consistent with filipin staining, an increase of lysosomal cholesterol content in *FABP7* KO cells compared with the wild-type (WT) control (Fig. 1 G).

We also measured intracellular cholesterol levels using a well-established probe consisting of the cholesterol-binding domain 4 of Perfringolysin O and the 6×His and EGFP tag at the N terminus (His_6-EGFP-D4H) (Maekawa and Fairn, 2015). Excess cholesterol was seen in lysosomes of *FABP7* KO cells but not of WT ones (Fig. 1, H and I). Together, these results suggest that FABP7 is involved in the lysosomal efflux of cholesterol.

FABP7 facilitates the egress of LDL-derived cholesterol from lysosomes

Cholesterol in the cell includes that from LDLs or from de novo biosynthesis (Brown and Goldstein, 1986; Ishitsuka et al., 2011). To determine the source of cholesterol accumulated in *FABP7* KO cells, we grew cells in the presence of fetal bovine serum (normal medium) as well as under the conditions where either lipoproteins were removed by ultracentrifugation (lipoprotein deficiency) or cholesterol biosynthesis was inhibited by lovastatin (endogenous cholesterol deficiency), followed by filipin staining to detect intracellular cholesterol contents. FABP7 depletion caused a sequestration of cholesterol in lysosomes of cells cultured in the normal medium as well as in the absence of endogenous cholesterol (Fig. 2, A, C, and D). However, under lipoprotein-deficient conditions, ablation of FABP7 was unable to induce cholesterol accumulation (Fig. 2, B and D) unless LDL was repleted (Fig. 2, E–G). Silencing of LDL receptor (LDLR) using siRNA (Fig. S2, A and B) markedly alleviated lysosomal cholesterol deposition in two lines of *FABP7* KO cells grown in normal medium (Fig. S2, C and D). These results suggest that the cholesterol conveyed by FABP7 out of lysosomes was derived from LDL.

To determine whether deficiency of FABP7 affects LDLR levels on the PM, we performed the cell surface biotinylation assay and found no differences in LDLR protein levels in either whole cell lysates or surface portion of WT cells and *FABP7* knockdown cells (Fig. S2 E). The internalization of Dil-LDL was similar between WT and *FABP7* KO cells (Fig. S2, F and G). These results suggest that cholesterol accumulation in lysosomes is not a result of increased LDL uptake by LDLR.

To investigate whether changes in lysosomal pH may cause cholesterol accumulation, we utilized LysoSensor Green to measure the pH value of lysosomes in *FABP7* KO cells. The fluorescence intensity of pH-sensitive LysoSensor Green puncta was not affected by FABP7 deficiency (Fig. S2, H and I).

FABP7 mediates cholesterol trafficking to the PM

Once LDL-derived cholesterol exits lysosomes, it is primarily directed to the PM and the ER (Das et al., 2014; Pfisterer et al., 2016; Infante and Radhakrishnan, 2017). The membrane contact sites between lysosome, peroxisome, and the ER mediate the non-vesicular transport of cholesterol from lysosomes to the ER (Chu et al., 2015; Xiao et al., 2019). To examine the effects of FABP7 deficiency on PM cholesterol levels, cells were depleted of cholesterol for 16 h, refed with 20 μg/ml LDL for various periods, followed by staining with the His_6-EGFP-D4H probe (Fig. 3 A). The EGFP fluorescence determined by flow cytometry was a

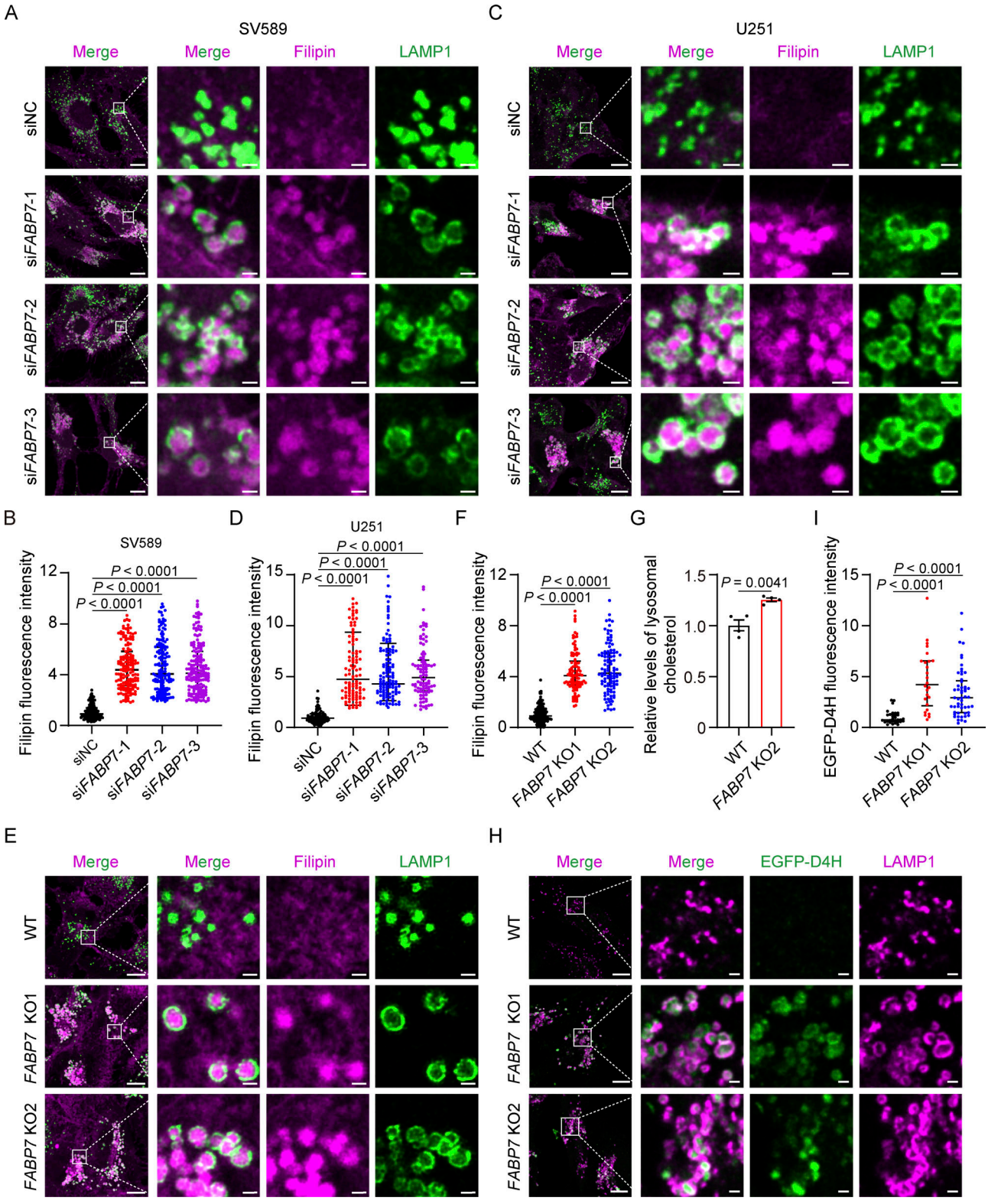

Figure 1. **FABP7 deficiency induces cholesterol accumulation in lysosomes. (A–D)** SV589 fibroblasts (A and B) and U251 cells (C and D) were transfected with the indicated siRNAs for 48 h, fixed, and stained with filipin (magenta) and the antibody against endogenous LAMP1 (green). Boxed areas are shown at a higher magnification on the right. Scale bars, 10 µm (main), 1 µm (inset). Relative fluorescence intensity of filipin in A and C was quantified by ImageJ and shown in B and D, respectively. Data are presented as median with interquartile range (n = 651 cells from three independent experiments in B, and n = 401 cells from three independent experiments in D). Mann–Whitney U test. Compared with cells transfected with scrambled control siRNA (NC, negative control). **(E)** Wild-type (WT) and two lines of *FABP7* knockout (KO) SV589 fibroblasts (*FABP7* KO1 and *FABP7* KO2) were fixed and stained with filipin (magenta) and the anti-LAMP1 antibody (green). Boxed areas are shown at a higher magnification on the right. Scale bars, 10 µm (main), 1 µm (inset). **(F)** Quantification of relative

fluorescence intensity of filipin in E. Data are presented as median with interquartile range (n = 356 cells from three independent experiments). Mann–Whitney U test. Compared with WT cells. **(G)** Relative cholesterol levels of lysosomes purified from WT and *FABP7* KO2 cells normalized to protein amounts. Data are presented as mean ± SEM (from four independent experiments). Student's unpaired two-tailed t test. Compared with WT cells. **(H)** WT and two lines of *FABP7* KO cells (*FABP7* KO1 and *FABP7* KO2) were fixed, breached with a liquid nitrogen pulse, stained with the purified recombinant His_6-EGFP-D4H protein (green) and the anti-LAMP1 antibody (magenta). Boxed areas are shown at a higher magnification on the right. Scale bars, 10 µm (main), 1 µm (inset). **(I)** Quantification of relative fluorescence intensity of His_6-EGFP-D4H protein in H. Data are presented as median with interquartile range (n = 110 cells from three independent experiments). Mann–Whitney U test. Compared with WT cells.

measure of PM cholesterol level. Compared with WT cells, *FABP7* KO cells showed a significant reduction in PM cholesterol following cholesterol depletion as well as after cholesterol repletion with total cholesterol levels unaltered (Fig. 3, B and C). The moderate decrease may be at least attributed to, first, the residual cholesterol on the PM, and second, the existence of other trafficking routes or STPs.

To ascertain that reduced PM cholesterol results from and not results in impaired cholesterol transport, WT and *FABP7* KO cells were treated with 1.5% 2-hydroxypropyl-β-cyclodextrin (HPCD) in the last 10 min of cholesterol depletion (Fig. 3 D). This treatment minimized the difference in PM cholesterol levels (Fig. 3 E, 0 h), and also created a concentration gradient that facilitated cholesterol transport from lysosomes to the PM. When LDL was repleted, *FABP7* KO cells still showed attenuated increases in PM cholesterol levels over time (Fig. 3 E). By contrast, lentivirus-mediated overexpression of *FABP7* significantly enhanced cholesterol levels in the PM (Fig. 3 F). Together, these results suggest that FABP7 promotes the trafficking of LDL-derived cholesterol from lysosomes to the PM.

To examine the effect of FABP7 on LDL cholesterol transport to the ER, we performed the sterol regulatory element-binding protein 2 (SREBP2) cleavage assay as previously described (Trinh et al., 2020) by first depleting WT and *FABP7* KO cells of cholesterol and then adding back increasing concentrations of LDL (1–30 µg/ml). The proteolytic cleavage of SREBP2, as evidenced by the generation of the nuclear form from the precursor form, in WT and *FABP7* KO cells was similarly inhibited by LDL (Fig. 3, G and H). Therefore, FABP7 deficiency barely affects the transportation of LDL-derived cholesterol to the ER.

Crystal structures of FABP7 in apo state and cholesterol bound-state

We next sought to solve the crystal structure of FABP7. The recombinant His_6-tagged FABP7 protein was expressed in *E. coli* and purified using the nickel beads. The endogenous lipids were removed from purified protein using a delipidation protocol as previously described (Balendiran et al., 2000). The apo state structure was solved at the resolution of 1.4 Å (Fig. 4 A). The structures of FABP7 in complex with cholesterol or 25-hydroxysterol (25-HC) were solved at a resolution of 2.7 Å and 2.6 Å, respectively (Fig. 4, B and C). The details of data collection and refinement are listed in Table S1. FABP7 is composed of three α helices and 10 antiparallel β-strands (Fig. 4, A–C). Cholesterol and 25-HC were found to be situated in the hydrophobic pocket of FABP7 in very similar conformations (Fig. 4, B and C). The water (apo) or sterol (cholesterol or 25-HC) inside was illustrated by the *2Fo-Fc* electron density map (Fig. S3, A–C).

FABP7 in complex with cholesterol shows a root-mean-square deviation of 0.229 Å across all atoms compared with the apo form (Fig. 4 D). The helical lid region of FABP7 is formed by the F58 residue, α2 and α3, and undergoes a conformational change upon cholesterol binding (Fig. 4 D). In the NMR structure of FABP7 (PDB code: 1JJX) (Rademacher et al., 2002), the F58 residue exhibits an open conformation in apo state. However, in the crystal structure, F58 adopts a closed conformation in the apo state and cholesterol- or 25-HC-bound state (Fig. 4 E). Such a highly dynamic nature of F58 and the lid may permit the entry or exit of sterol molecules.

The sterol-binding pocket of FABP7 contains several hydrophobic residues, including F17, M21, P39, A76, M116, and L118, around the tetracyclic ring of sterol (Fig. 4 F and Fig. S3 D). Two hydrophilic residues, R127 and Y129, form hydrogen bonds with the 3β-hydroxyl group of the sterol molecule (Fig. 4 F and Fig. S3 D).

Identification of the key residues in FABP7 mediating cholesterol transport

To determine the key residues required for FABP7-mediated cholesterol transport, we prepared the plasmid expressing Flag-tagged WT FABP7 or those with the abovementioned residues mutated to alanine, glycine, or phenylalanine as indicated, and examined their rescuing effects on cholesterol accumulation in *FABP7* KO cells (Fig. 5 A). The fluorescence of R127I/A/L mutants was weak probably due to low expression, and the R127 mutation was therefore not evaluated. Re-expression of FABP7 carrying the F17A and L118A mutations could effectively remove excess cholesterol from *FABP7* KO cells as that of WT FABP7 did, indicating that F17 and L118 residues are not required for FABP7-mediated cholesterol egress from lysosomes (Fig. 5, B and C). By contrast, all other mutants failed to alleviate cholesterol accumulation caused by FABP7 deficiency, suggesting that M21, P39, F58, A76, M116, and Y129 are all indispensable for cholesterol mobilization by FABP7.

To determine whether FABP7 mutants that failed to promote intracellular cholesterol transport are indeed defective in cholesterol binding, we employed the ^{3}H-cholesterol binding assay with purified FABP7 variants. The wild-type FABP7 protein showed a dissociation constant of 3.04 ± 0.78 µM (Fig. 5 D). Mutations in the residues critical for intracellular cholesterol trafficking (M21A, P39A, F58A, A76G, M116A, and Y129F) impaired the binding of ^{3}H-labeled cholesterol to FABP7, though the effect of A76G was not statistically significant (Fig. 5 E).

FABP7 can bind several fatty acids, including oleic acid, docosahexaenoic acid, palmitic acid, and arachidonic acid (Liu et al., 2010). To determine whether fatty acids may compete for cholesterol binding, we performed the competitive binding

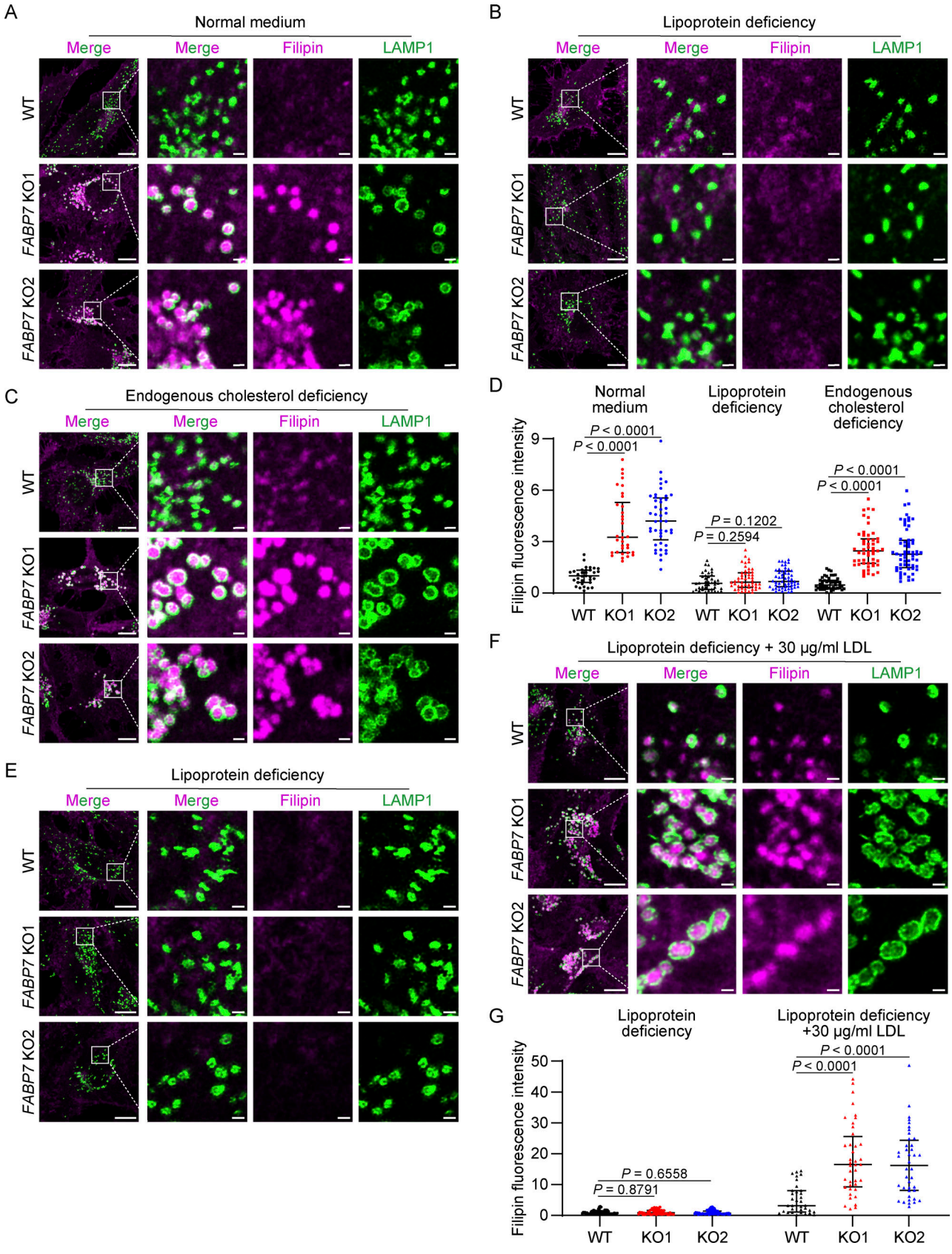

Figure 2. **FABP7 mediates the egress of low-density lipoprotein (LDL)-derived cholesterol from lysosomes. (A–C)** WT and two lines of *FABP7* KO cells (*FABP7* KO1 and *FABP7* KO2) were incubated in normal medium (10% fetal bovine serum, A), lipoprotein-deficient medium (5% lipoprotein-deficient serum, B), or endogenous cholesterol-deficient medium (10% fetal bovine serum with 1 µM lovastatin and 10 µM mevalonate, C) as indicated for 16 h. Cells were fixed and

stained with filipin (magenta) and the anti-LAMP1 antibody (green). Boxed areas are shown at a higher magnification on the right. Scale bars, 10 µm (main), 1 µm (inset). **(D)** Quantification of relative fluorescence intensity of filipin in A–C. Data are presented as median with interquartile range (n = 418 cells from three independent experiments). Mann–Whitney U test. Compared with WT cells grown under the same conditions. **(E and F)** WT and two lines of *FABP7* KO cells (*FABP7* KO1 and *FABP7* KO2) were incubated in lipoprotein-deficient medium (E) or lipoprotein-deficient medium supplemented with 30 µg/ml LDL (F) for 16 h and stained with filipin (magenta) and the anti-LAMP1 antibody (green). Boxed areas are shown at a higher magnification on the right. Scale bars, 10 µm (main), 1 µm (inset). **(G)** Quantification of relative fluorescence intensity of filipin in E and F. Data are presented as median with interquartile range (n = 295 cells from three independent experiments). Mann–Whitney U test. Compared with WT cells grown under the same conditions.

assay using ^{3}H-cholesterol and fatty acids which are known to be the endogenous ligands for FABP7. Cholesterol was also included as a positive control. The results showed that all the tested fatty acids could compete with ^{3}H-cholesterol for FABP7 binding (Fig. 5 F). Consistent with other studies (Balendiran et al., 2000; Liu et al., 2010), oleic acid was the most potent ligand and showed a dose-dependent competing effect (Fig. 5, F and G). These results suggest that cholesterol and fatty acids bind competitively to FABP7.

Among the six FABP7 mutants, M21A, P39A, and Y129F were defective in binding either cholesterol or oleic acid (Fig. 5, E and H). However, mutations in the A76 residue but not F58 or M116—which resides at the lid of hydrophobic pocket and forms the hydrophobic interaction with the tetracyclic ring of sterol, respectively (Fig. 4)—greatly reduced FABP7 binding to oleic acid. These results suggest that FABP7 has overlapping yet different binding sites for cholesterol and oleic acid.

FABP7 can efficiently transfer cholesterol in vitro

We next sought to investigate whether FABP7 can directly transfer cholesterol using the DHE transport assay as previously described (Wang et al., 2019). The donor liposomes (Ld) were made of DOPC (92.5 mol%), DNS-PE (2.5 mol%), and DHE (5 mol %), whereas the acceptor liposomes (La) contained DOPC only. The transfer of DHE from donor to acceptor liposomes was revealed by decreased fluorescence resonance energy transfer signal between DHE and DNS-PE on Ld (Fig. 6 A). To ascertain whether DHE—a natural fluorescent analog of cholesterol—is a legitimate probe to measure cholesterol transport, we added increasing amounts (5, 10 and 20 mol%) of cholesterol into the donor liposomes and found FABP7-mediated transportation of DHE was dose-dependently inhibited by cholesterol (Fig. 6, B and C). These results suggest that DHE can mimic cholesterol in the context of our study.

ORP2 is reported to participate in cholesterol transport to the PM (Wang et al., 2019). The purified FABP7 protein promoted DHE transport to an extent similar to the purified OSBP-related domain (ORD) of ORP2 (Fig. 6, D and E). However, F58A and Y129F mutations almost completely abrogated the amount of DHE transferred as well as the initial DHE transport rate (Fig. 6, F and G). Consistent with the finding that L118 is dispensable for intracellular cholesterol transport (Fig. 5, B and C), the L118A mutant could transport DHE as efficiently as the WT protein did (Fig. 6, F and G).

To exclude the possibility that FABP7 may induce liposome fusion, we measured liposome radius before and after the recombinant FABP7 protein was added to the in vitro DHE transport system using the dynamic light scattering assay (Wilhelm et al., 2017). The results showed that neither the mean radius nor size distribution of liposomes was altered by the wild-type FABP7 protein or the F58A, L118A, or Y129F mutants (Fig. 6, H and I), suggesting that FABP7 does not induce liposome fusion.

FABP3 and FABP8 can bind and transport cholesterol

There have been 10 human FABPs identified so far and each has tissue-specific distribution and distinct ligand preference (Haunerland and Spener, 2004; Smathers and Petersen, 2011). Despite significant variations in amino acid sequences (Richieri et al., 1994), all FABP family members exhibit highly conserved β-barrel tertiary structures that can accommodate a hydrophobic ligand in a non-covalent, reversible manner, thereby increasing the ligand's solubility in the aqueous cytoplasm (Storch and Corsico, 2008). To test whether other FABP family members can bind and transport cholesterol, we depleted each one using shRNAs (Fig. S4 A) and detected robust cholesterol accumulation in lysosomes of *FABP3* and *FABP8* knockdown SV589 cells (Fig. 7, A and B). Silencing of FABP3 or FABP8 also caused lysosomal cholesterol accumulation in U251 (Fig. S4, B–D) and MA10 cells (Fig. S4, E–H). By contrast, cholesterol was barely accumulated in those depleted of FABP1, 2, 4, 5, 6, 9, or 12, suggesting these FABPs were not involved in cholesterol transport. Depletion of FABP3 and FABP8 failed to alter LDLR protein levels (Fig. S2 E), LDL uptake (Fig. S4, I and J), or lysosomal pH (Fig. S4, K and L).

Except for M116, all the residues (M21, P39, F58, A76, and Y129) responsible for cholesterol binding and transport are conserved in FABP3, FABP7, and FABP8 (Fig. S4 M). To determine whether these three FABPs function redundantly to mediate cholesterol transport, we knocked down FABP3 and FABP8 using shRNAs in *FABP7* KO cells. NPC1 knockdown was the positive control. Compared with a single depletion of FABP3, FABP7, or FABP8, combined depletion of all three FABPs resulted in a much more pronounced cholesterol accumulation phenotype (Fig. 7, C and D). We further purified lysosomes from single- or triple-depleted cells for cholesterol level measurement. In line with the filipin results, lysosomal cholesterol levels were significantly higher when FABP3, FABP7, or FABP8 were all absent (Fig. 7, E and F). These results suggest that the total amount of FABP3, 7, and 8 determined the transportation efficiency.

The binding affinity of purified FABP3 and FABP8 proteins for ^{3}H-cholesterol or ^{3}H-oleic acid was evaluated as well. FABP6 has a very low affinity for oleic acid (Gong et al., 1994; Fujita et al., 1995), and an equal amount of FABP6 was included as a negative control. Compared with FABP7, FABP3 showed modestly yet significantly reduced binding affinity for cholesterol, whereas FABP8 bound cholesterol as potently as FABP7 (Fig. 8 A). Both FABP3 and FABP8 could bind oleic acid avidly (Fig. 8 B). Oleic acid was able to compete with cholesterol for binding with FABP3 or FABP8 (Fig. 8, C and D). In vitro, FABP3 and FABP8 could transfer DHE as efficiently as FABP7 (Fig. 8, E and F).

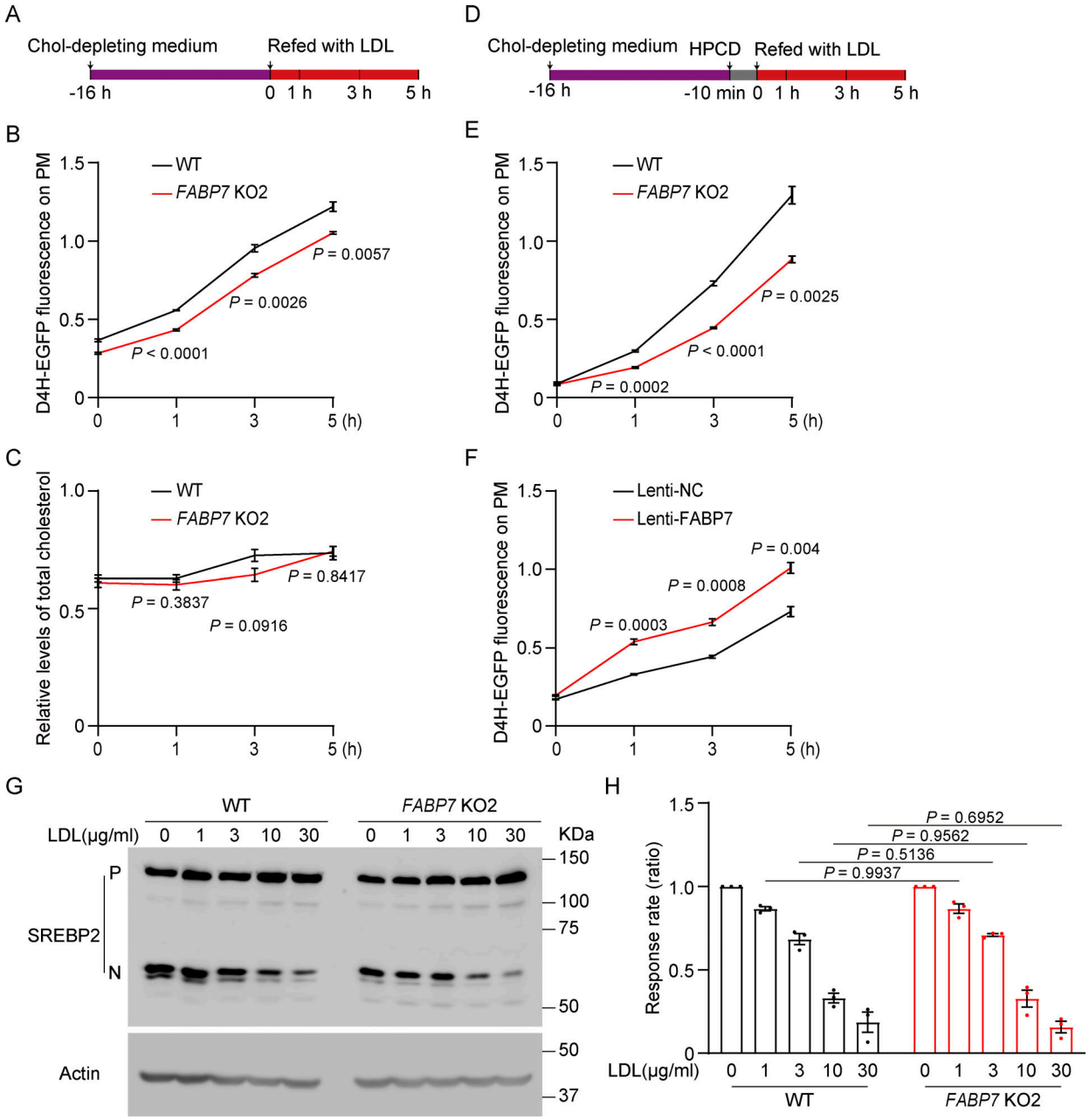

Figure 3. **FABP7 promotes LDL cholesterol transport to the PM. (A–C)** WT and *FABP7* KO2 SV589 cells were incubated in the cholesterol (Chol)-depleting medium for 16 h and refed with cholesterol-depleting medium containing 20 μg/ml LDL for the indicated periods as shown in A. Cells were then stained with the His_6-EGFP-D4H probe and subjected to flow cytometry for EGFP fluorescence measurement (B) or harvested for biochemical analysis of cholesterol levels (C). The EGFP fluorescence intensity of WT and *FABP7* KO2 cells cultured in normal medium is defined as 1. Data are presented as mean ± SEM (from three biological replicates). Student's unpaired two-tailed *t* test. Compared with WT cells refed with LDL for the same periods of time. **(D and E)** WT and *FABP7* KO2 SV589 cells were depleted of cholesterol as in A, and in the last 10 min of 16 h cholesterol depletion was treated with 1.5% 2-hydroxypropyl-β-cyclodextrin (HPCD). Cells were then refed with cholesterol-depleting medium containing 20 μg/ml LDL for the indicated periods as shown in D, and stained with the His_6-EGFP-D4H probe and subjected to flow cytometry for EGFP fluorescence measurement. The EGFP fluorescence intensity of WT and *FABP7* KO2 cells cultured in normal medium is defined as 1. Data are presented as mean ± SEM (from three biological replicates). Student's unpaired two-tailed *t* test. Compared with WT cells refed with LDL for the same periods of time. **(F)** SV589 cells infected with lentivirus (Lenti-) expressing negative control (NC) or FABP7 were treated as in D, and EGFP fluorescence intensity was quantified. The EGFP fluorescence intensity of WT and *FABP7* KO2 cells cultured in normal medium is defined as 1. Data are presented as mean ± SEM (from three biological replicates). Student's unpaired two-tailed *t* test. Compared with cells infected with lentivirus expressing negative control (NC) and refed with LDL for the same periods of time. **(G and H)** WT and *FABP7* KO2 cells were depleted of cholesterol for 16 h and treated with the indicated concentrations of LDL for 5 h at 37°C. Cells were subjected to SREBP2 cleavage analysis. **(G)** Representative immunoblots showing SREBP2 cleavage. P, the precursor form of SREBP2; N, the nuclear form of SREBP2. **(H)** The ratio of the densitometry of the nuclear SREBP2 over that of both nuclear and precursor forms of SREBP2. The ratio of cells without LDL repletion was defined as 1. Data are presented as mean ± SEM (from three independent experiments). Student's unpaired two-tailed *t* test. Compared with WT cells refed with LDL at the same concentrations. Source data are available for this figure: SourceData F3.

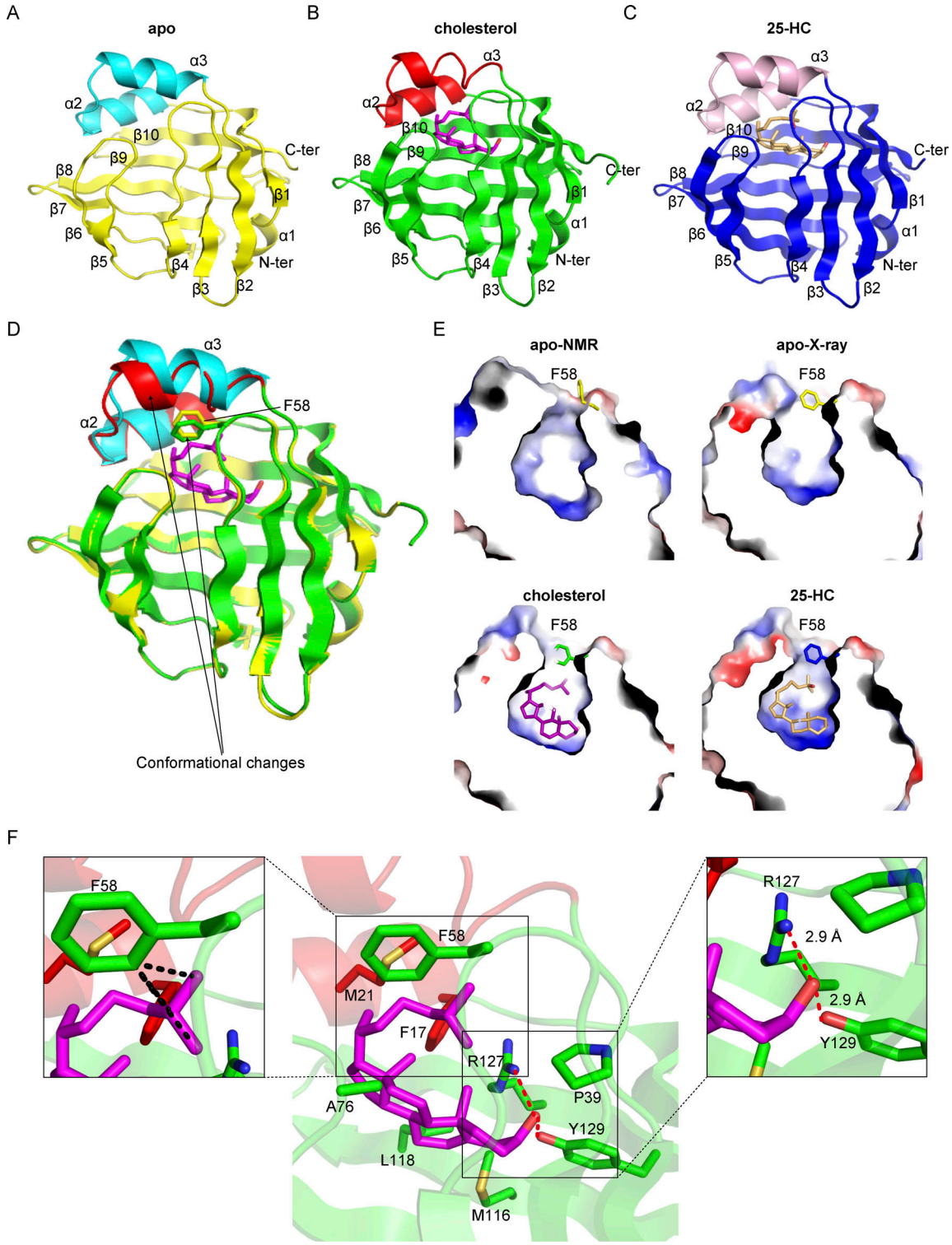

Figure 4. **Crystal structures of human FABP7 protein. (A–C)** Overall structure of FABP7 protein in apo state (A) and ligand-binding state (B and C). Cholesterol is highlighted as magenta sticks in B, and 25-hydroxycholesterol (25-HC) is highlighted as light orange sticks in C. **(D)** Superposition of apo (yellow) and cholesterol-bound (green) FABP7 structures. **(E)** The nuclear magnetic resonance (NMR) or x-ray analysis showing empty or ligand-bound FABP7 with the F58 residue in open and closed conformations. **(F)** Detailed view of FABP7 interacting with cholesterol (magenta sticks). Hydrogen bonds formed between FABP7 and the hydroxyl group of cholesterol are denoted by red dashed lines. The hydrophobic interactions between FABP7 F58 and cholesterol are shown by black dashed lines. Key residues for cholesterol binding are indicated.

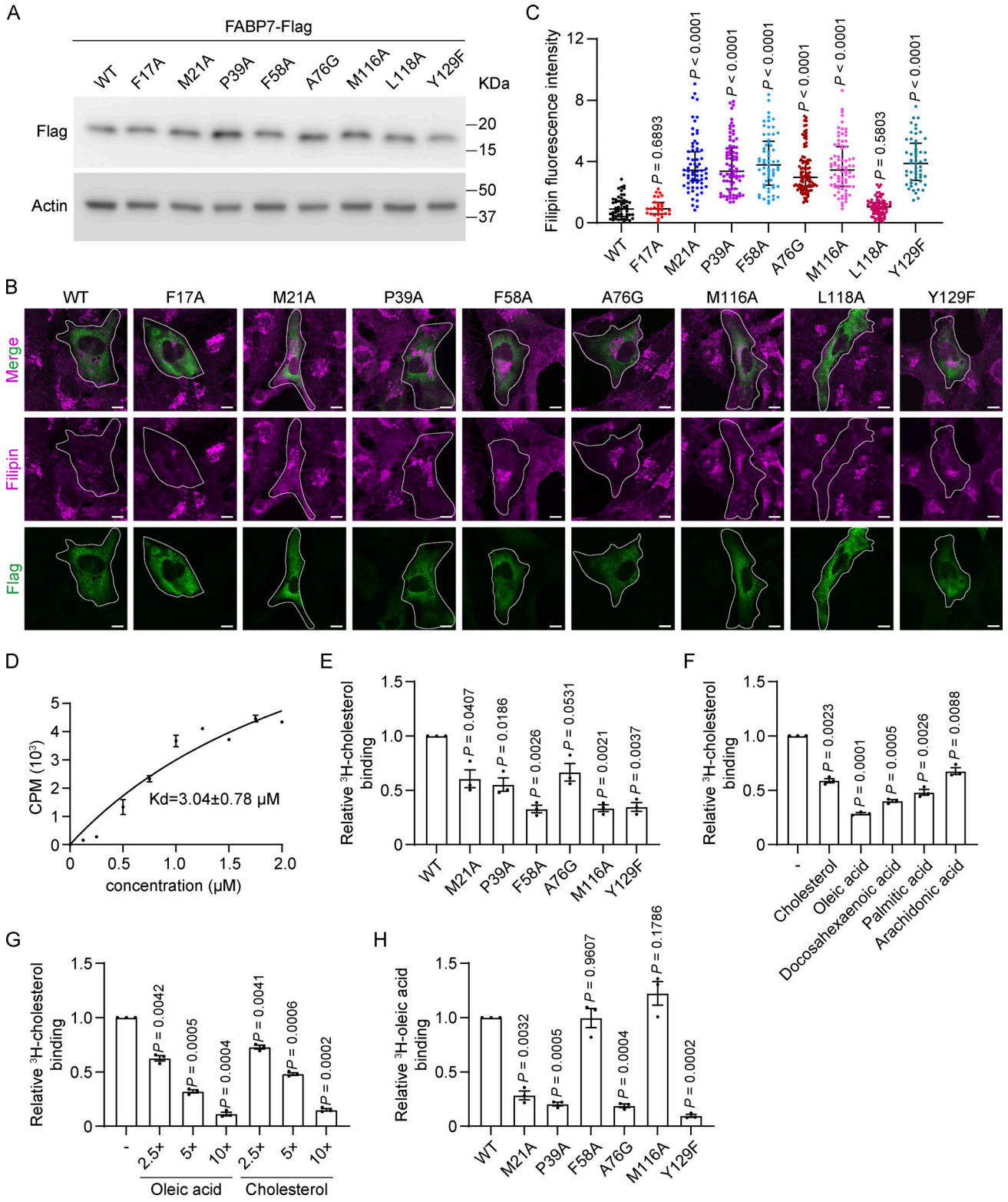

Figure 5. **Identification of FABP7 key residues involved in cholesterol transport and binding. (A–C)** *FABP7* KO2 cells were transfected with the indicated plasmids expressing various FABP7 mutants tagged with Flag for 48 h and harvested. **(A)** Immunoblotting analysis showing the expression of indicated FABP7 mutants. **(B)** Cells were fixed and stained with filipin (magenta) and the antibody against Flag (green). Scale bars, 10 μm. **(C)** Quantification of relative fluorescence intensity of filipin in B. The filipin fluorescence intensity of *FABP7* KO2 cells transfected with the plasmid expressing wild-type (WT) FABP7 is defined as 1 and used as the reference for comparison. Data are presented as median with interquartile range (n = 583 cells from three independent experiments). Mann–Whitney U test. **(D)** The cholesterol binding activities of FABP7 protein. Data are presented as mean ± SEM (from three independent experiments). **(E)** Binding of ^{3}H-cholesterol to WT FABP7 recombinant protein and the indicated mutants. Equal amounts of proteins were used in the reaction. CPM measured for ^{3}H-cholesterol bound to WT FABP7 protein is defined as 1 and used as the reference for comparison. Data are presented as mean ± SEM (from

three independent experiments). Student's unpaired two-tailed *t* test with Welch's correction. **(F)** Binding of ^{3}H-cholesterol to FABP7 in the presence of different fatty acids. CPM measured for ^{3}H-cholesterol bound to FABP7 in the absence of (–) the indicated competitors is defined as 1 and used as the reference for comparison. Data are presented as mean ± SEM (from three independent experiments). Student's unpaired two-tailed *t* test with Welch's correction. **(G)** Binding of ^{3}H-cholesterol to FABP7 in the presence of increasing concentrations of oleic acid or cholesterol. CPM measured for ^{3}H-cholesterol bound to FABP7 in the absence of (–) the indicated competitors is defined as 1 and used as the reference for comparison. Data are presented as mean ± SEM (from three independent experiments). Student's unpaired two-tailed *t* test with Welch's correction. **(H)** Binding of ^{3}H-oleic acid to WT FABP7 and the indicated mutants. Equal amounts of proteins were used in the reaction. CPM measured for ^{3}H-oleic acid bound to WT FABP7 is defined as 1 and used as the reference for comparison. Data are presented as mean ± SEM (from three independent experiments). Student's unpaired two-tailed *t* test with Welch's correction. Source data are available for this figure: SourceData F5.

FABP8 has been recently demonstrated to bind PIP_2 (Abe et al., 2021). To determine whether FABP3, 7, and 8 could exchange DHE for PIP_2, we performed the DHE transport assay using the acceptor liposomes consisting of 96 mol% DOPC and 4 mol% $PI(3,4)P_2$, $PI(3,5)P_2$, $PI(4,5)P_2$ or not in the absence or presence of each FABP protein. Both FABP3 and FABP8 could support DHE transport to the acceptor liposomes without or with any of the three PIP_2 species (Fig. S5, A, B, E, and F). However, PIP_2 was found to inhibit FABP7-mediated DHE transport, with the most significant effect by $PI(4,5)P_2$ (Fig. S5, C and D).

We also incorporated PIP_2 onto the donor liposomes. All three species of PIP_2 hampered the total amounts of DHE transport by FABP3, 7 or 8 (Fig. S5, G, I, and K). The rate of DHE transferred by FABP3 was more or less the same regardless of PIP_2 used (Fig. S5 H), whereas that by FABP7 or FABP8 was significantly diminished by $PI(3,5)P_2$ and $PI(4,5)P_2$ (Fig. S5, J and L). We therefore conclude that FABP3, FABP7, or FABP8 are unlikely to mediate sterol/PIP_2 exchange.

Discussion

STPs can facilitate sterol desorption from the membranes by decreasing the extraction energy barrier (Dittman and Menon, 2017) as well as promoting sterol movement across the cytoplasm by shielding the hydrophobic molecules within the internal cavity (Wong et al., 2019). Most STPs identified so far fall into three large families, with each possessing distinct sterol-binding domains (Luo et al., 2019). In this study, we reported that FABP3, FABP7, and FABP8 are involved in cholesterol egress from lysosomes. FABP7 harbors a cholesterol-binding pocket and selectively delivers cholesterol to the PM. FABP3, FABP7, and FABP8 can bind cholesterol and transfer its analog in vitro. These results suggest that FABPs represent a new class of STPs.

The binding of cholesterol to FABPs is not totally unprecedented. FABP1 (a.k.a. liver FABP) can bind cholesterol analogs or derivatives in vitro, and cholesterol binding competitively displaces one of the two fatty acids from FABP1 (Martin et al., 2009; Nemecz and Schroeder, 1991). Cholesterol is also predicted to be the ligand for FABP8 by docking simulations using the high-resolution crystal structure (Majava et al., 2010). We hereby show that FABP3, FABP7, and FABP8 are not only able to bind cholesterol but also to transport DHE between liposomes in vitro. More importantly, these three FABPs are responsible for cholesterol egress from lysosomes (Fig. 7). The binding of cholesterol is a prerequisite for its trafficking by FABP7 since the mutants defective in cholesterol binding cannot revert cholesterol accumulation caused by FABP7 depletion (Fig. 5). The residues crucial for cholesterol binding and transport include the F58 residue at the lid region, the hydrophobic residues of the sterol-binding pocket (M21, P39, A76, and M116), and the Y129 residue that forms hydrogen bonds with the 3β-hydroxyl group of sterol (Fig. 4). However, the F17 and L118 residues—two hydrophobic ones in the sterol-binding pocket—only form a few (7 and 2 van der Waals contacts, respectively; cutoff for van der Waals contacts calculation is 4.5 Å) interactions with cholesterol, therefore barely contributing to intracellular cholesterol trafficking, given that the neighboring amino acids could provide sufficient interactions to stabilize the binding of sterol molecules. The importance of these above residues in cholesterol binding and transport is further highlighted by their conservation in FABP3, FABP7, and FABP8 (Fig. S4 M). It is speculated that cholesterol is similarly buried within FABP3 and FABP8.

Our study identifies FABP7 as a cytosolic protein that can interact with lysosomes to mediate cholesterol transport from lysosomes to the PM. ORP1S and ORP2 have been reported to mediate cholesterol transport from endosomes/lysosomes to the PM (Zhao et al., 2020; Wang et al., 2019). Furthermore, a vesicular process involving the Rab8a- and CD63-positive LY-related organelles contribute as well (Kanerva et al., 2013). Owing to the presence of these multiple routes, the effect of FABP7 deficiency on PM cholesterol levels is unlikely to be all-to-none. Of note, unlike ORP2, which can bind sterol and $PI(4,5)P_2$ and exchange the two, FABP7 binds and transfers fatty acids, such as oleic acid and docosahexaenoic acid (Balendiran et al., 2000), and fatty acids compete with cholesterol for FABP7 binding (Fig. 5). We also demonstrate that FABP7 is unlikely to be a counter-exchanger of DHE and PIP_2 (Fig. S5). Hence, FABP7 and ORP2 seem to be two independent transporters for directional cholesterol trafficking from lysosomes to the PM. How FABP7 is targeted to lysosomes and the PM and whether FABP7 may mediate cholesterol trafficking to places other than the PM or the ER are yet to be determined. The destinations cholesterol is delivered to by FABP3 and FABP8 warrant further investigation.

FABP3 and FABP7 are brain-expressed FABPs with close implications for neuropsychiatric disorders and some neurodegenerative diseases. Multiple genetic variants of *FABP3* and *FABP7* are exclusively detected in schizophrenia and autism spectrum disorder patients (Shimamoto et al., 2014). Disturbed levels of FABP3 and FABP7 have been observed in the serum and/or cerebrospinal fluid of patients with schizophrenia, autism spectrum disorder, and some neurodegenerative diseases (Mollenhauer et al., 2007; Sepe et al., 2018; Teunissen et al., 2011). In mice, knockout of *Fabp3* and *Fabp7* produces

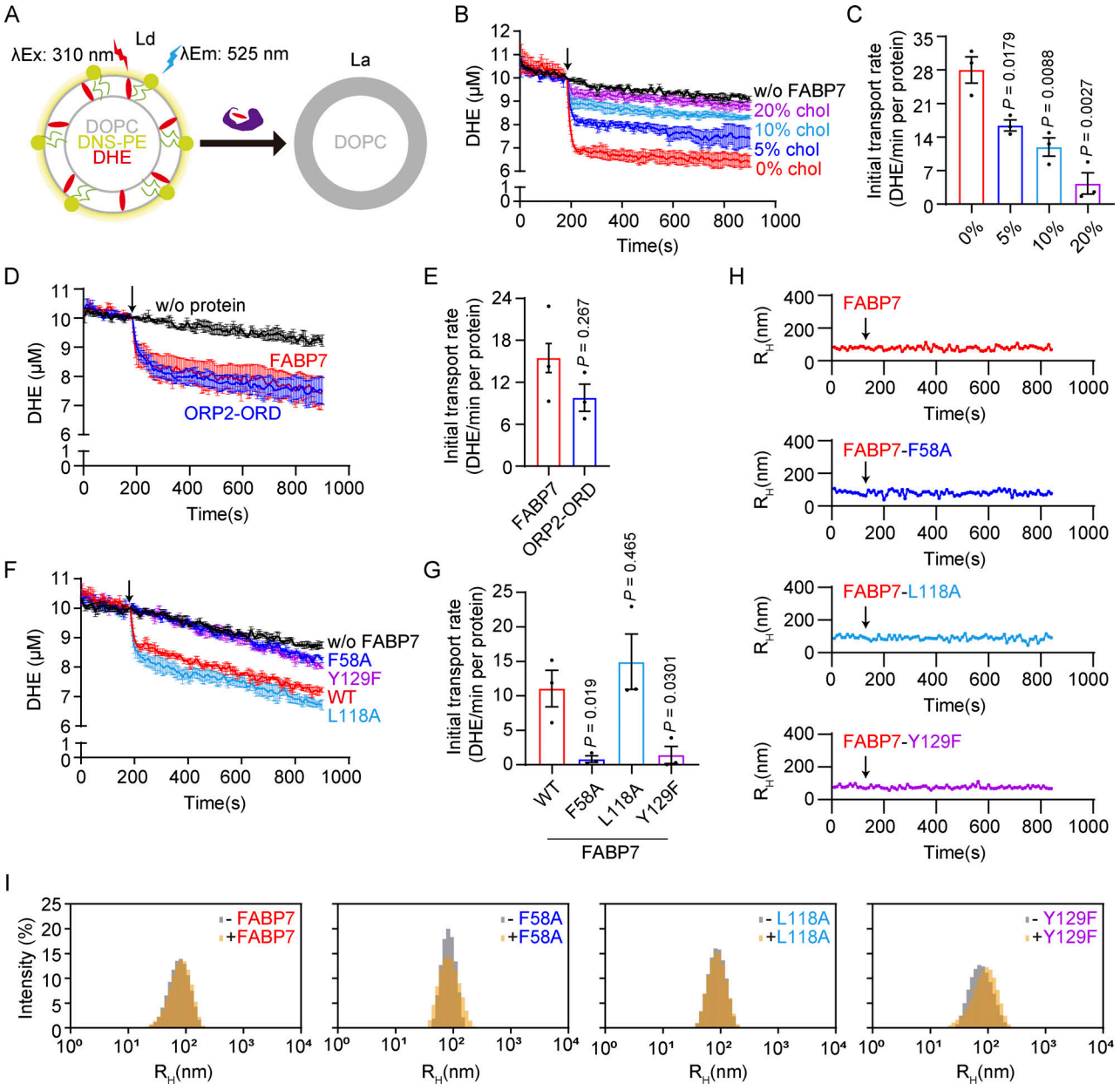

Figure 6. **FABP7 transfers cholesterol analog in vitro. (A)** Schematic illustration of in vitro dehydroergosterol (DHE) transport assay. Donor liposomes (Ld) are made of 92.5 mol% 1,2-dioleoyl-sn-glycero-3-phosphocholine (DOPC), 5 mol% DHE and 2.5 mol% 1,2-dioleoyl-sn-glycero-3-phosphoethanolamine-N-(5-dimethylamino-1-naphthalenesulfonyl (DNS-PE). Acceptor liposomes (La) only contain DOPC. Ld and La were incubated at 25°C for 3 min and FRET between DHE and DNS-PE (λEx: 310 nm, λEm: 525 nm) was recorded. The purified proteins were then added to a final concentration of 0.5 μM and incubated for 12 min. The transport of DHE from Ld to La is determined by the diminution in FRET between DHE and DNS-PE. **(B and C)** The effect of increasing concentrations of cholesterol (0, 5, 10 or 20 mol%) in donor liposomes on DHE transport by FABP7. Arrow indicates when FABP7 protein was added. Initial transport rates were quantified in C. Data are presented as mean ± SEM (from three independent experiments). Student's unpaired two-tailed *t* test. Compared with the donor liposomes without cholesterol. **(D and E)** Comparison of the effects of purified FABP7 and ORP2-ORD proteins on DHE transfer. Arrow indicates when the indicated proteins were added. Initial transport rates were quantified in E. Data are presented as mean ± SEM (from three independent experiments). Student's unpaired two-tailed *t* test. Compared with initial transport rates of DHE by FABP7 protein. **(F and G)** Comparison of the effects of FABP7 WT and mutant proteins on DHE transfer. Arrow indicates when the indicated proteins were added. Initial transport rates were quantified in G. Data are presented as mean ± SEM (from three independent experiments). Student's unpaired two-tailed *t* test. Compared with initial transport rates of DHE by wild-type (WT) FABP7 protein. **(H and I)** Liposome aggregation in F was assessed by dynamic light scattering. The acceptor liposomes (La, containing DOPC only, 50 μM total lipids) were mixed with the donor liposomes (Ld, containing 92.5 mol% DOPC, 5 mol% DHE, and 2.5 mol% DNS-PE, 50 μM total lipids). The size distribution of the initial liposome suspension was assessed by acquiring a first set of about 12 autocorrelation curves. The indicated proteins were then added manually and mixed thoroughly. **(H)** The mean radius over time. Arrow indicates when the indicated proteins were added. **(I)** The size distribution before (gray) and after the reaction (colored).

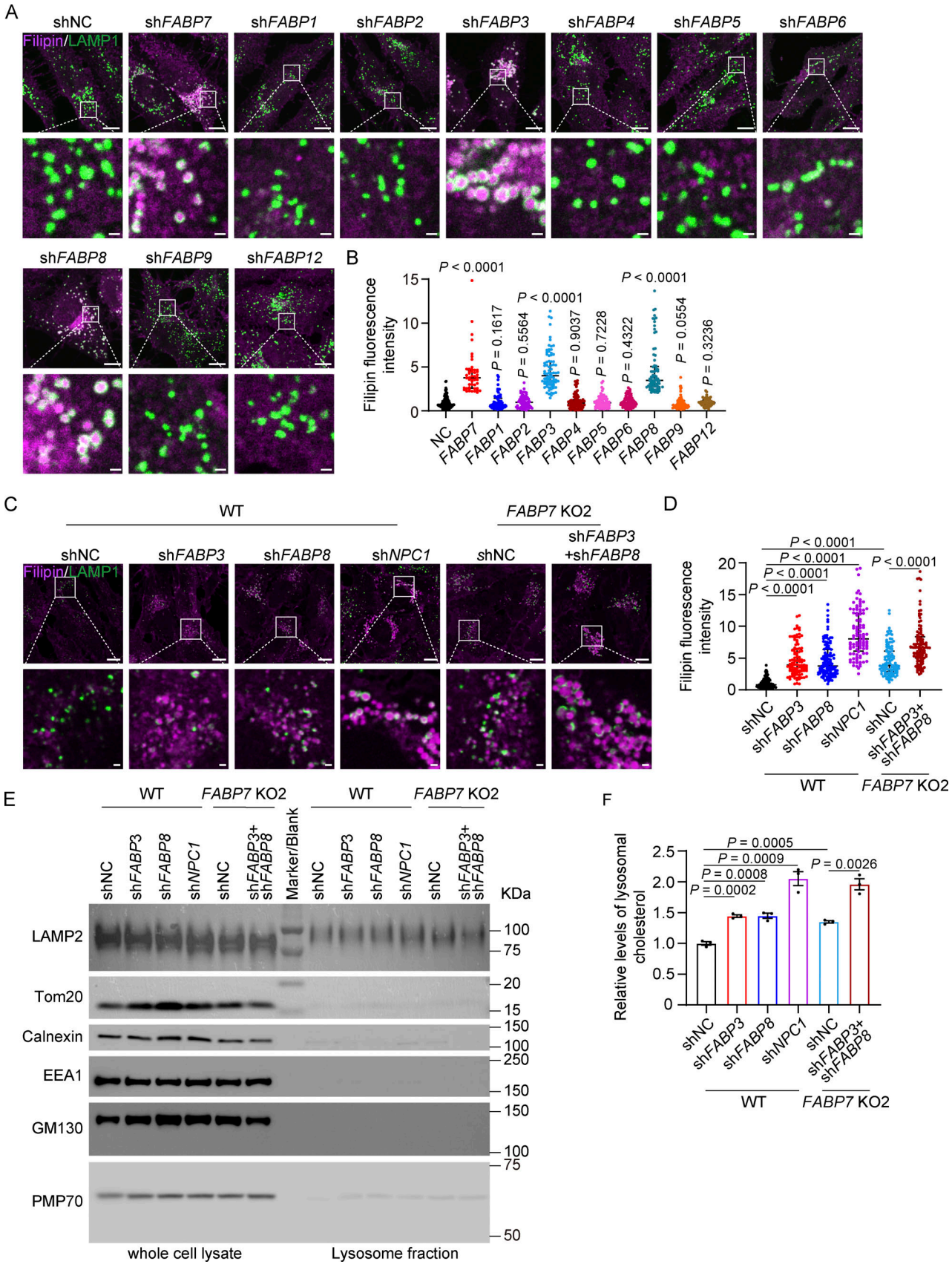

Figure 7. **FABP3 and FABP8 are critical for lysosomal cholesterol egress. (A and B)** SV589 fibroblasts were infected with lentivirus expressing indicated shRNAs, fixed and stained with filipin (magenta) and the anti-LAMP1 antibody (green). Boxed areas are shown at a higher magnification on the bottom. Scale

bars, 10 µm (main), 1 µm (inset). The relative fluorescence intensity of filipin was quantified in B. The filipin fluorescence intensity of cells infected with lentivirus expressing scrambled control shRNA (NC, negative control) is defined as 1 and used as the reference for comparison. Data are presented as median with interquartile range (n = 885 cells from three independent experiments). Mann–Whitney U test. **(C and D)** WT and *FABP7* KO2 SV589 fibroblasts infected with lentivirus expressing indicated shRNAs were fixed and stained with filipin (magenta) and the anti-LAMP1 antibody (green). Boxed areas are shown at a higher magnification on the bottom. Scale bars, 10 µm (main), 1 µm (inset). The relative fluorescence intensity of filipin was quantified in D. The filipin fluorescence intensity of wild-type (WT) cells infected with lentivirus expressing scrambled control shRNA (NC, negative control) is defined as 1 and used as the reference, except for *FABP7* KO2 cells infected with lentivirus expressing shRNA targeting FABP3 and FABP8. The filipin fluorescence intensity of *FABP7* KO2 cells infected with lentivirus expressing scrambled control shRNA (NC, negative control) is the reference when comparing *FABP7* KO2 cell groups. Data are presented as median with interquartile range (n = 728 cells from three independent experiments). Mann–Whitney U test. **(E)** Indicated cells were treated as in C, and lysosomes were purified and subjected to immunoblotting analysis. **(F)** Relative cholesterol levels of purified lysosomes normalized to protein amounts. The lysosomal cholesterol levels in WT cells infected with lentivirus expressing scrambled control shRNA (NC, negative control) is defined as 1 and used as the reference, except for *FABP7* KO2 cells infected with lentivirus expressing shRNA targeting FABP3 and FABP8. The lysosomal cholesterol levels of *FABP7* KO2 cells infected with lentivirus expressing scrambled control shRNA (NC, negative control) are the reference when comparing *FABP7* KO2 cell groups. Data are presented as mean ± SEM (from three independent experiments). Student's unpaired two-tailed t test. Source data are available for this figure: SourceData F7.

behavioral phenotypes reminiscent of schizophrenia and autism (Shimamoto et al., 2014). Notably, altered cholesterol distribution and cholesterol dyshomeostasis in the brain are also implicated in autistic spectrum disorders (Woods et al., 2012), schizophrenia (Jensen et al., 2017), Alzheimer's disease, and NPC disease (Nixon, 2004; Wolozin, 2004; Xiao et al., 2021a). It is possible that cholesterol accumulation as a result of FABP deficiency may also contribute to the pathogenesis of the abovementioned diseases. For example, impaired formation and maturation of neuronal dendrites seen in *Fabp7* knockout mice (Ebrahimi et al., 2016) can be caused by cholesterol accumulation in astrocytes that otherwise feed neurons with cholesterol. Future work is needed to elucidate the functional significance of FABP-mediated cholesterol trafficking at the systemic level.

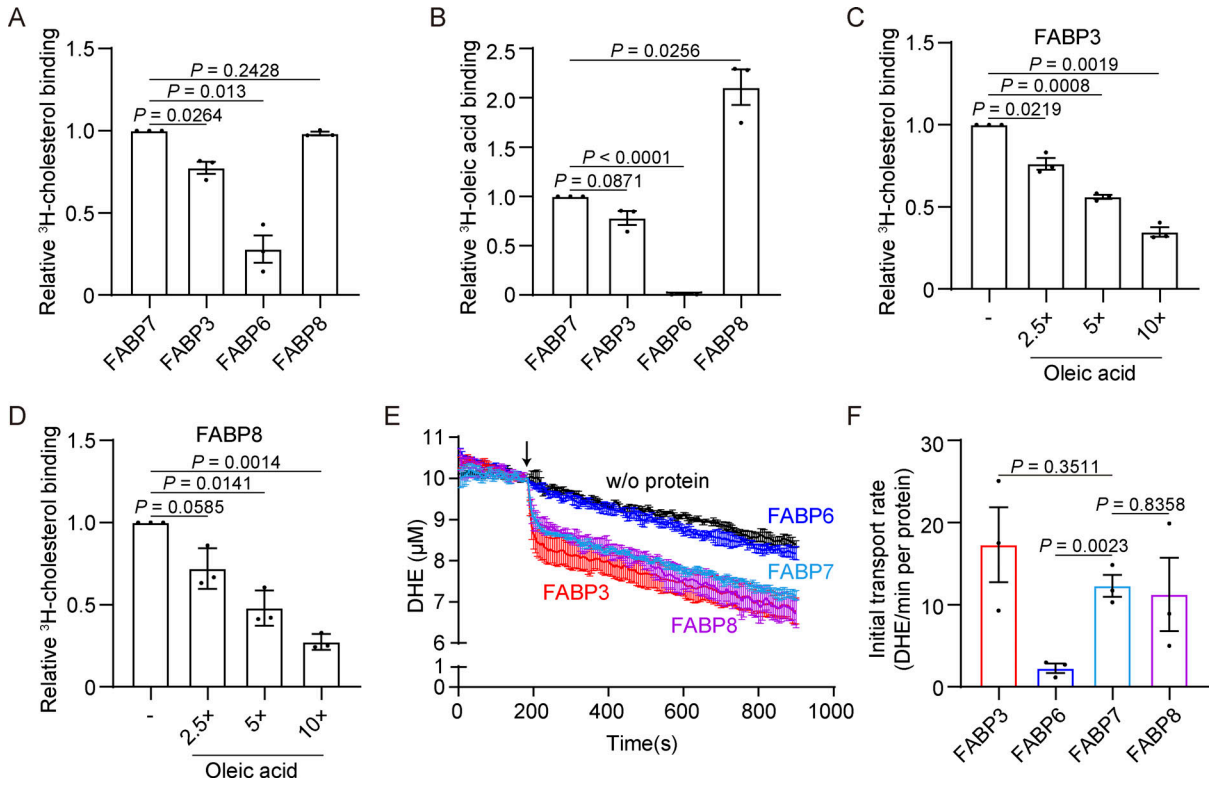

Figure 8. **FABP3 and FABP8 bind and transfer cholesterol in vitro. (A)** Binding of ^{3}H-cholesterol to the indicated FABP proteins. Equal amounts of proteins were used in the reaction. CPM measured for ^{3}H-cholesterol bound to WT FABP7 is defined as 1 and used as the reference for comparison. Data are presented as mean ± SEM (from three independent experiments). Student's unpaired two-tailed t test with Welch's correction. **(B)** Binding of ^{3}H-oleic acid to the indicated FABP proteins. Equal amounts of proteins were used in the reaction. CPM measured for ^{3}H-oleic acid bound to WT FABP7 is defined as 1 and used as the reference for comparison. Data are presented as mean ± SEM (from three independent experiments). Student's unpaired two-tailed t test with Welch's correction. **(C and D)** Binding of ^{3}H-cholesterol to FABP3 (C) and FABP8 (D) in the presence of increasing concentrations of oleic acid. CPM measured for ^{3}H-cholesterol bound to FABP3 (C) and FABP8 (D) in the absence of oleic acid is defined as 1 and used as the reference for comparison. Data are presented as mean ± SEM (from three independent experiments). Student's unpaired two-tailed t test with Welch's correction. **(E and F)** Comparison of the effects of indicated proteins on DHE transfer. Arrow indicates when proteins were added. Initial transport rates were quantified in F. Data are presented as mean ± SEM (from three independent experiments). Student's unpaired two-tailed t test. Compared with initial transport rates of DHE by FABP7 protein.

Taken together, this study demonstrates that FABPs are a new class of STPs involved in intracellular cholesterol trafficking. Modulating the ability of FABPs to transport cholesterol could serve as a potential approach to treat neuropsychiatric disorders and neurodegenerative diseases.

Materials and methods

Reagents

Filipin (F9765), dehydroergosterol (DHE) (E2634), sodium mevalonate (41288), and 25-hydroxycholesterol (H1015) were from Sigma-Aldrich. Cholesterol (T0760), oleic acid (T2O2668), docosahexaenoic acid (T5369), arachidonic acid (T4129), and palmitic acid (T2908) were obtained from TargetMol. Lovastatin (purity ≥98.5%, HPLC) was from Shanghai Pharm Valley. Digitonin (300410) was from Millipore. ^{3}H-cholesterol (NET139) and ^{3}H-oleic acid (NET289) were from PerkinElmer. DOPC (850375), brain PI(4,5)P_2 (840046), 18:1/18:1 PI(3,4)P_2 (850153), 18:1/18:1 PI(3,5)P_2 (850154), and DNS-PE (810330) were from Avanti Polar Lipids. Ni-NTA agarose (30230) was from Qiagen. FuGENE HD transfection reagent (E2312) was from Promega. EZ-Link Sulfo-NHS-LC-Biotin (21335) was from Thermo Fisher Scientific. Human Dil-LDL (20614ES76) and LysoSensor Green DND-189 (40768ES50) were from Yeasen. Ponceau S (A610437) and CHAPS (A600110) were from Sangon Biotech. Lipoprotein-deficient serum (LPDS) and LDL were prepared from newborn calf serum by ultracentrifugation and from human blood by density gradient centrifugation, respectively, in our laboratory.

Plasmids

The coding sequences of human FABP3, FABP6, FABP7, FABP8, and the domain 4 (amino acids 391–500) of Perfringolysin O bearing the D434S mutation (D4H) were synthesized by Tsingke Biotechnology. The coding sequence of FABP7 with a Flag-tagged to the C terminus was cloned into the pcDNA3 (V011312; Novo-Pro) or pLVX-IRES-Puro vector (632183; Clontech). The coding sequences of FABP3, FABP6, FABP7, FABP8, and ORP2-ORD (amino acids 41–480) were cloned into the pET28a vector (69864; Novagen) with a 6×His tag at the C terminus. The coding sequence of D4H was cloned into the pET28a vector with a 6×His tag and an EGFP tag at the N terminus. All mutants were made by site-directed mutagenesis using KOD Hot Start DNA polymerase (KOD-401; TOYOBO) and verified by Sanger sequencing.

Antibodies

The primary antibodies were as follows: mouse anti-EEA1(610457; BD Biosciences), mouse anti-LAMP1 (H4A3; Developmental Studies Hybridoma Bank), rabbit anti-PMP70 (PA1-650; Thermo Fisher Scientific), rabbit anti-FLAG tag (20543-1-AP; Proteintech), mouse anti-FLAG tag (F3165; Sigma-Aldrich), mouse anti-β-actin (A1978; Sigma-Aldrich), rabbit anti-Tom20 (11802-1-AP; Proteintech), mouse anti-LAMP2 (sc-18822; Santa Cruz Biotechnology), rabbit anti-calnexin (10427-2-AP; Proteintech), mouse anti-GM130 (610823; BD Transduction Laboratories), and rabbit anti-FABP8 (12717-1-AP; Proteintech). The mouse anti-SREBP2 antibody had been generated from hybridoma cell line 1D2 (CRL-2545; ATCC) in our laboratory as previously described (Xiao et al., 2021b).

The rabbit anti-FABP3 antibody was prepared by Wuhan DIA-AN Biotechnology, China. The coding sequence of the human *FABP3* gene with a 6×His tag at the C terminus was cloned into the pcDNA3.1 (V790-20; Invitrogen) and expressed by HEK293F cells (R79007; Thermo Fisher Scientific) grown at 37°C with 5% CO_2, followed by purification using the column containing Ni-NTA agarose. The purified FABP3 protein was immunized into three rabbits, with each injected four times at an interval of 28, 14, and 14 d. Freund's complete adjuvant (F5881; Sigma-Aldrich) was used in the first injection and Freund's incomplete adjuvant (F5506; Sigma-Aldrich) was used for the rest of the injections. 3 d after the fourth injection, antiserum titer was determined by enzyme-linked immunosorbent assay. The rabbit with the highest titer was sacrificed on the 64th day since the first injection. The antiserum was applied onto CNBr-activated Sepharose 4B (17-0430-01; GE Health) coupled to 1 mg purified FABP3 protein. The antibody was eluted with the glycine HCl buffer (pH 2.5), followed by dialysis and concentration.

The rabbit anti-LDLR antibody had been generated in our laboratory as previously described (Wang et al., 2021; Zhou et al., 2023). The coding sequence corresponding to human LDLR (amino acids 98–147) was cloned into the pGEX-6p-1 (27-4597-01; Amersham) and expressed by *E. coli* BL21(DE3) that were grown in Luria-Bertani broth containing 0.1 mM isopropylthio-β-galactoside at 18°C overnight. The protein was purified using the Glutathione Sepharose 4 Fast Flow beads (17-5132-02; Cytiva) and immunized into rabbits as described above.

Primary antibodies were used at the dilution of 1:500 for immunofluorescent staining and 1:1,000 for immunoblotting. Alexa Fluor 555 donkey anti-mouse (1:1,000; A31570), Alexa Fluor 555 donkey anti-rabbit (1:1,000; A31572), Alexa Fluor 488 donkey anti-mouse (1:1,000; A11001), and Alexa Fluor 488 donkey anti-rabbit (1:1,000; A11008) secondary antibodies were from Invitrogen. Horseradish peroxidase-conjugated goat anti-mouse (115-035-003) and goat anti-rabbit (111-035-144) secondary antibodies were from Jackson ImmunoResearch Laboratories.

Cell culture

HEK293T (CRL-3519) and MA-10 (CRL-3050) cells were from ATCC. SV589 cells were a kind gift from the Laboratory of Brown & Goldstein. U251 cells were from the National Collection of Authenticated Cell Cultures. SV589, HEK293T, and U251 cells were cultured in Dulbecco's modified Eagle's medium (DMEM) containing 100 U/ml penicillin and 100 μg/ml streptomycin sulfate (Medium A) supplemented with 10% fetal bovine serum (FBS). MA-10 cells were grown in DMEM/Ham's F-12 supplemented with 5% FBS and 2.5% heat-inactivated horse serum, 100 U/ml penicillin, and 100 μg/ml streptomycin sulfate. The lipoprotein-deficient medium was Medium A supplemented with 5% LPDS. The endogenous cholesterol-deficient medium was Medium A supplemented with 10% FBS, 1 μM lovastatin, and 10 μM mevalonate. The cholesterol-depleting medium was Medium A supplemented with 5% LPDS, 1 μM lovastatin, and 10 μM mevalonate. Cells were grown as a monolayer at 37°C with 5% CO_2.

No further authentication of the cell lines was performed before use. No test for mycoplasma contamination was performed.

Generation of *FABP7* knockout cell line

The sgRNAs were cloned into the pX330-U6-Chimeric-bb-CBh-hSpCas9 vector (42230; Addgene). The plasmids were then transfected together with puromycin-resistant PLKO.1 (10878; Addgene) into SV589 cells for 24 h. Cells were subjected to 4 μg/ml puromycin selection for a few days until the cells without PLKO.1 transfection all died. The puromycin-resistant cells were diluted to ensure single-cell seeding in 96-well plates. The single colony formed was identified by Sanger sequencing. The full sequences of sgRNAs are listed in Table S2.

Production of shRNA lentiviral particles

The shRNAs were designed using BLOCK-iT RNAi Designer website and cloned into the pLKO.1 vector. HEK293T cells were plated at a density of 3×10^6 cells per 10-cm plate and transfected with 3 μg shRNA-containing pLKO.1, 2.25 μg psPAX2 (12260; Addgene) and 0.75 μg pMD2.G (12259; Addgene) using LPEI. The medium was replaced 6 h after transfection and collected 48 h later. The full sequences of shRNAs are listed in Table S2.

RNA interference

Duplexes of siRNA were synthesized by Ribobio. The siRNAs were transfected into SV589 cells as indicated in the figure legends using Lipofectamine RNAiMAX according to the manufacturer's instructions. The full sequences of siRNAs are listed in Table S2.

Purification of recombinant proteins

BL21 (DE3) *E. coli* cells were transformed with the plasmids and grown at 37°C for 3–4 h until the OD_{600} value reached 0.6. Cells were induced to produce protein with 0.1 mM isopropylthio-β-galactoside overnight at 18°C. After spinning down at 6,760 *g* for 5 min, cells were resuspended and incubated in the lysis buffer (20 mM Tris-HCl, pH 7.4, and 200 mM NaCl) containing 1 mg/ml lysozyme and 1 mM phenylmethylsulfonyl fluoride on ice for 30 min. Cells were sonicated and lysates were treated with 5 μg/ml DNase I on ice for 30 min. After centrifugation at 27,000 *g* for 30 min, supernatants were collected and incubated with the Ni-NTA Agarose beads at 4°C for 4 h.

For FABP-His_6 proteins, beads were washed with buffer A (20 mM imidazole, 20 mM Tris-HCl, pH 7.4, 200 mM NaCl) and proteins were eluted with buffer B (500 mM imidazole, 20 mM Tris-HCl, pH 7.4, 200 mM NaCl). Proteins were finally dialyzed in a buffer containing 20 mM Tris-HCl, pH 7.4, 200 mM NaCl, and 1 mM DTT overnight at 4°C and stored at −80°C.

For His_6-EGFP-D4H protein, beads were washed with low imidazole buffer (40 mM imidazole, 500 mM NaCl, 20 mM Na_3PO_4, pH 7.4) and the protein was eluted with high imidazole buffer (500 mM imidazole, 500 mM NaCl, 20 mM Na_3PO_4, pH 7.4). Protein was finally dialyzed in PBS overnight at 4°C and stored in 10% glycerol at −80°C.

Filipin staining

Cells were fixed with 4% paraformaldehyde (PFA) for 30 min at room temperature and then incubated with 1×PBS containing 1% bovine serum albumin (BSA), 50 μg/ml filipin, and primary antibodies (1:500) for 2 h at room temperature. After PBS washes, cells were incubated with secondary antibodies (1:1,000) containing 50 μg/ml filipin for 1 h at room temperature.

Cholesterol labeling with D4H

For immunostaining analysis, cells were fixed with 4% PFA for 10 min at room temperature and permeabilized in a liquid nitrogen bath for 30 s. After blocking with 1% BSA in PBS for 1 h, cells were incubated with the purified recombinant His_6-EGFP-D4H protein (20 μg/ml in 1% BSA) for 2 h. Cells were then washed twice with PBS, re-fixed with 4% PFA for 10 min, and incubated with primary and secondary antibodies as described above.

For flow cytometry analysis, cells were trypsinized and incubated with the purified recombinant His_6-EGFP-D4H protein (20 μg/ml in 1% BSA) for 40 min at 4°C. Cells were then fixed with 4% PFA for 30 min at 4°C, rinsed, and subjected to flow cytometry analysis using a CytoFlex (BECKMAN COULTER) and FlowJo v10 software.

Immunofluorescence staining of FABP7

Cells on coverslips were permeabilized in a liquid nitrogen bath for 30 s or 0.005% digitonin diluted in DMEM containing 0.3 M sucrose for 5 min. After PBS washes, cells were fixed with 4% PFA for 30 min, permeabilized with 0.2% Triton X-100, blocked in 1% BSA for 1 h, and incubated with primary and secondary antibodies as described above. Nuclei were counterstained with DAPI (1:1,000).

Immunoblotting analysis

Cells were harvested and lysed in the RIPA buffer (50 mM Tris-HCl, pH 8.0, 150 mM NaCl, 2 mM $MgCl_2$, 1.5% NP-40, 0.1% SDS, and 0.5% sodium deoxycholate) plus protease inhibitors. The protein concentrations of lysates were quantified using a BCA kit (23225; Thermo Fisher Scientific). Samples were mixed with the 4× loading buffer (150 mM Tris-HCl, pH 6.8, 12% SDS, 30% glycerol, 6% 2-mercaptoethanol and 0.02% bromophenol blue) and boiled for 10 min at 95°C, or the 4×loading buffer plus the membrane solubilization buffer (62.5 mM Tris-HCl, pH 6.8, 15% SDS, 8 M urea, 10% glycerol, and 100 mM DTT) and incubated for 30 min at 37°C. The equal amounts of samples were subjected to SDS-PAGE, transferred to PVDF membranes, blocked with 5% non-fat milk in Tris-buffered saline (TBS) containing 0.1% Tween 20 (TBST), and incubated with primary antibodies overnight at 4°C. After TBST washes, blots were incubated with secondary antibodies (1:5,000) diluted in TBST supplemented with 5% non-fat milk for 1 h at room temperature. Blots were developed using a Pierce ECL Plus Western blotting substrate kit (32132; Thermo Fisher Scientific) and visualized under a Tanon-5200 chemiluminescent imaging system.

SREBP2 processing assay

Cells were grown in the cholesterol-depleting medium for 16 h and treated with the indicated concentrations of LDL for 5 h. Cells were then lysed in RIPA buffer plus protease inhibitors and subjected to immunoblotting analysis using the anti-SREBP2 antibody. Densitometry of SREBP2 proteins was qualified by ImageJ and normalized to that of β-actin.

Quantitative real-time PCR (qPCR)

RNA was extracted with Trizol Reagent (Sigma-Aldrich) and reversely transcribed into cDNA using M-MLV Reverse Transcriptase (Promega). QPCR was administered by the Hieff qPCR SYBR Green Master Mix (Monad) and analyzed on a Bio-Rad CFX96 apparatus. The RNA expression levels were calculated using the ΔΔCt method.

Liposome preparation

DOPC, DNS-PE, and DHE were solubilized in chloroform. The donor liposomes (Ld) consisted of 92.5 mol% DOPC, 2.5 mol% DNS-PE, and 5 mol% DHE (200 μM total lipids for DHE transport assay and 50 μM total lipids for the dynamic light scattering assay). The acceptor liposomes (La) consisted of 100 mol% DOPC (200 μM total lipids for DHE transport assay, and 50 μM total lipids for the dynamic light scattering assay). Cholesterol or 4 mol% of PIP_2 may be added as indicated, with a corresponding reduction in DOPC. Lipids were pipetted into a round bottom flask and dried in a rotary evaporator. Lipid films were resuspended and hydrated in HKM buffer (50 mM HEPES, pH 7.2, 120 mM potassium acetate, 1 mM $MgCl_2$). After 10 freezing–thawing cycles with liquid nitrogen, suspensions were extruded through a 100-nm pore polycarbonate filter using a mini-extruder (Avanti Polar Lipids). Liposomes were stored at 4°C in the dark and used within 2 d.

DHE transport assay

A total of 560 μl La was mixed with 30 μl of Ld and incubated at 25°C for 3 min. Purified protein (10 μl) was added at a final concentration of 0.5 μM. DHE transport assay was performed by monitoring the DNS-PE signal at 525 nm (bandwidth 20 nm) upon DHE excitation at 310 nm (bandwidth 10 nm). The decrease in FRET signal between DHE and DNS-PE on Ld was converted into the amount of DHE (in μM) transferred from Ld to La using the formula $10 * [(F–F_0)/(F_{max} – F_0)]$, where F_{max} and F represent signals before and after the addition of proteins, respectively, and F_0 represents the signal measured with liposomes containing DOPC and DNS-PE only. Measurements were obtained in a PerkinElmer LS55 fluorimeter equipped with a cylindrical quartz cuvette.

Preparation of FABP7 protein for crystallography study

The purified FABP7 was diluted to 35 ml with 10 mM Tris (pH 8.0). The diluted protein was delipidated by extracting 35 ml of protein solution three times with 14 ml of diisopropyl ether: n-butanol (3:2) for 30 min with gentle shaking. The protein was concentrated to 1 ml in 10 mM Tris (pH 8.0) and was then dissolved in the 7 M guanidine HCl solution (7 M Guanidine, 10 mM sodium acetate, 10 mM EDTA, pH 4.2) at room temperature overnight. The dissolved protein was refolded by rapid dilution in 100 mM Tris (pH 8.0), 2 mM EDTA, 400 mM L-Arginine HCl, 5 mM reduced glutathione, and 0.5 mM oxidized glutathione for 48 h at 4°C. For cholesterol or 25-HC bound FABP7, 10 mM cholesterol or 25-HC was added during the refolding. The refolded mixture was dialyzed for 12 h against 20 volumes of 10 mM Tris (pH 8.0). The dialyzed protein was purified by the Ni-NTA Agarose as described above.

Crystallization and x-ray data collection

The dialyzed protein was concentrated at 10 mg/ml for crystallization. Crystals were obtained at 4°C using the sitting-drop vapor-diffusion method from 0.1 M Bis-Tris (pH 5.5), 25% (wt/vol) PEG 3350. Before data collection, the crystals were transferred into the crystallization buffer containing 20% (wt/vol) glycerol and flash-cooled in liquid nitrogen. The diffraction data sets were collected at Shanghai Synchrotron Radiation Facility on the beam line BL17U1/BL18U1/BL19U1. Diffraction data were processed with the program iMosflm 6 (Battye et al., 2011) and scaled by Aimless Pointless in the CCP4 software suite 7 (Winn et al., 2011). The structures were determined by molecular replacement using the program PHASER, and the structure of FABP7 (PDB code: 5URA) was used as a search model (McCoy et al., 2007). The models from the molecular replacement were built with the program COOT (Emsley and Cowtan, 2004) and subsequently subjected to refinement by the program PHENIX.refine (Adams et al., 2002). Data collection, processing, and refinement statistics are summarized in Table S1. For apo structure and cholesterol-bound structure, one asymmetric unit contains one copy of the molecule and two copies for 25-HC bound structure. All structure figures were prepared using PyMOL.

Dynamic light scattering

All the experiments were performed at 25°C in a Zetasizer Nano ZSP (Malvern Instruments) equipped with a 633-nm He–Ne laser and operated at an angle of 173°. The sample in HKM buffer initially contained donor and acceptor liposomes. A first set of about 12 autocorrelation curves was acquired to assess the size distribution of the initial liposome suspension. Protein was then added manually and mixed thoroughly, and the kinetics of aggregation was followed by acquiring one autocorrelation curve every 10 s. The data were analyzed by the Zetasizer v7.11 software (Malvern Instruments) by fitting the autocorrelation functions with the assumption that the size distribution is a simple Gaussian function, thus giving an average radius.

Radiolabeled ligand binding assay

The cholesterol-binding assay was performed as previously described (Winkler et al., 2019) with slight modifications as follows. In brief, 150 nM of delipidated human His-tagged FABP7 proteins was incubated with ^{3}H-cholesterol premixed with unlabeled cholesterol in the 1:4 ratio to a final concentration of 125, 250, 500, 750, 1,000, 1,250, 1,500, 1,750, and 2,000 nM in a binding buffer (20 mM Tris-HCl, pH 7.4, and 200 mM NaCl) containing 0.004% Triton X-100. For analysis of FABP7 mutants and FABP family proteins binding with cholesterol or oleic acid, 150 nM of proteins was incubated with ^{3}H-ligand premixed with unlabeled ligands (1:4) to a final concentration of 1.5 μM. Control was made for each of the above-stated concentrations in the absence of protein. The values obtained in the control were later subtracted from the measurements with protein present. Each reaction was adjusted to 200 μl with binding buffer plus 0.05% CHAPS and gently vortexed and incubated at 25°C for 3 h. The nickel beads were then washed in binding buffer plus 0.05% CHAPS, and 40 μl nickel beads were transferred to each reaction

with 400 µl buffer above mentioned. After incubation at 25°C for 1 h with constant mixing, the beads were pelleted by centrifuge at 1,000 *g* for 5 min and washed four times with 1 ml of binding buffer plus 0.05% CHAPS. After the last wash, the beads were collected by centrifugation at 1,000 *g* for 1 min and the proteins were eluted with 500 µl elution buffer (20 mM Tris-HCl, pH 7.4, 200 mM NaCl, 300 mM imidazole) and quantified by liquid scintillation counting. In each experiment, all tubes received the same amounts of ethanol.

Radiolabeled sterol competition assay

The competition assays were performed similarly to the radiolabeled ligand binding assay. In brief, 150 nM of delipidated human His-tagged FABP7 proteins was incubated with ^{3}H-cholesterol premixed with unlabeled cholesterol in the 1:4 ratio to a final concentration of 1.5 µM. The competitors, such as 7.5 µM (5×) of either unlabeled cholesterol or fatty acids, and 3.75 µM (2.5×), 7.5 µM (5×) or 15 µM (10×) of either unlabeled cholesterol or oleic acid, were solubilized in ethanol and diluted into separate tubes with a binding buffer containing 0.004% Triton X-100. All tubes were added ethanol to ensure the same total amounts of ethanol.

Cell surface biotinylation assay

Cells were rinsed twice with ice-cold PBS and incubated with 1 mg/ml EZ-Link Sulfo-NHS-LC-Biotin in PBS for 30 min at 4°C. At the end of the labeling reaction, 100 mM glycine was added and incubated for 10 min at 4°C. Three washes with glycine were performed to quench the excess biotin completely. Cells were then washed with PBS and lysed in lysis buffer (50 mM HEPES, 150 mM NaCl, 1% NP-40, pH 7.4) plus protease inhibitors. One-fifth of the cell lysates was saved and the rest was incubated with Neutravidin agarose beads for 2 h at 4°C to pull down biotinylated cell surface proteins. After incubation, beads were washed five times with lysis buffer. Beads were mixed with the 1× loading buffer containing a final concentration of 2 mM biotin and 20 mM DTT and boiled for 10 min at 95°C. Both the samples representing total and surface protein were analyzed by immunoblotting.

Lysosome purification

The purification of lysosome was performed by using lysosome isolation kits (LYSISO1; Sigma-Aldrich) according to the manufacturer's instructions. In brief, cells were homogenized in extraction buffer and spun down serially at 1,000 *g* for 10 min and 20,000 *g* for 20 min. Then, the pellets were suspended in extraction buffer and placed on 8%, 12%, 16%, 19%, 22.5%, and 27% (vol/vol) iodixanol gradients and then centrifuged at 150,000 *g* for 4 h. Fractions were collected from the top to the bottom and the purest lysosomes were pooled together to extract lipids for measuring the level of cholesterol. Organelle purity was assessed by examining for the presence of organelle-specific markers in all components of equal volumes.

Lysosomal cholesterol measurement

The lysosomal cholesterol was extracted with chloroform–methanol (2:1). The organic phase was dried under nitrogen and dissolved with ethanol. Free lysosomal cholesterol was measured with an Amplex Red Cholesterol Assay Kit (A12216; Invitrogen). In brief, the lipids were incubated with the Amplex Red reagent/HRP/cholesterol oxidase working solution according to the manufacturer's instructions at 37°C for 45 min. The fluorescence in a fluorescence microplate reader was detected with excitation at 545 nm and emission at 590 nm.

LysoSensor staining

Cells were plated in a 35-mm glass bottom dish. LysoSensor Green DND-189 at a final concentration of 1 µM was added to the cell culture medium and incubated at 37°C for 1 h. After two washes with PBS, the medium was replaced, and cells were subjected for live-cell imaging. The fluorescence intensity of LysoSensor was quantified by Fiji Image J software.

Microscope image acquisition

Immunofluorescence images were acquired under a Leica Biosystems SP8 laser-scanning confocal microscope equipped with 405, 488, and 552 nm lasers, 63×/1.3 oil objective, and HyD and PMT detectors at room temperature. Images were exported with LAS X software (Leica) under identical settings.

Quantification and analysis of immunofluorescent images

The immunofluorescence intensity of filipin, EGFP-D4H, DiI-LDL, and LysoSensor Green was measured using Fiji ImageJ software. The relative immunofluorescence intensities were defined as the ratios of mean values of individual intensities in experimental conditions normalized to those of control groups. Colocalization coefficients were determined using the Coloc 2 plugin of Fiji ImageJ as an index for the ratio of colocalization between FABP7 and organelle markers to the number of FABP7.

Statistical analysis

Data were analyzed using the GraphPad Prism 8 software. All the data were first analyzed for normality using the Shapiro–Wilk test. The normally distributed data are presented as mean ± SEM, and Student's unpaired two-sided *t* test was used for comparison between the two groups. The Welch's correction was applied if the homogeneity of variances was violated. The non-normally distributed data are presented as median with interquartile range, and Mann–Whitney U test was used. Sample sizes, statistical tests, and P values (unless <0.0001) for each experiment are stated in the relevant figures and figure legends.

Online supplemental material

Fig. S1 shows the subcellular localization of FABP7 and characterization of FABP7 knockdown and knockout in cultured cells. Fig. S2 shows that LDLR-mediated LDL uptake provides cholesterol for FABP7-mediated transport. Fig. S3 shows the crystal structure of apo and ligand-binding FABP7. Fig. S4 shows cholesterol accumulation in the cells lacking FABP3 or FABP8. Fig. S5 shows that PIP_2 does not enhance DHE transport by FABPs. Table S1 shows data collection and refinement statistics. Table S2 shows the full sequences of oligos used in this study.

Data availability

The data that support the findings of this study are available within the paper and its supplementary files. Source data used to

generate figures containing Western blots have been provided in this study. The atomic coordinates and structure factors for the reported crystal structures have been deposited in the PDB with the accession codes 6L9O (FABP7 apo), 8IVL (FABP7_Cho), and 8IVF (FABP7_25-HC).

Acknowledgments

This work was supported by grants from the National Natural Science Foundation of China (32021003, 32293203, and 91954203), Natural Science Foundation of Hubei Province for Distinguished Young Scholars (2023AFA050), and Ministry of Science and Technology of China (2018YFA0800700). B.-L.S. acknowledges the support from the Tencent Foundation through the XPLORER PRIZE.

Author contributions: B.-L. Song and J. Luo conceived the project and directed the research. X.-X. Fang and Z.-C. Sheng conducted the cell biology experiments and lipid transport experiments. P. Wei and K. Zhao performed the x-ray crystallography, bioinformatics, and structural modeling studies. B.-L. Song, J. Luo, L. Yin, X.-X. Fang, and P. Wei wrote the paper.

Disclosures: The authors declare no competing interests exist.

Submitted: 16 November 2022
Revised: 22 March 2023
Accepted: 18 January 2024

References

Abe, M., A. Makino, M. Murate, F. Hullin-Matsuda, M. Yanagawa, Y. Sako, and T. Kobayashi. 2021. PMP2/FABP8 induces PI(4,5)P_2-dependent transbilayer reorganization of sphingomyelin in the plasma membrane. *Cell Rep.* 37:109935. https://doi.org/10.1016/j.celrep.2021.109935

Adams, P.D., R.W. Grosse-Kunstleve, L.W. Hung, T.R. Ioerger, A.J. McCoy, N.W. Moriarty, R.J. Read, J.C. Sacchettini, N.K. Sauter, and T.C. Terwilliger. 2002. PHENIX: Building new software for automated crystallographic structure determination. *Acta Crystallogr. D Biol. Crystallogr.* 58:1948–1954. https://doi.org/10.1107/S0907444902016657

Ayalew, M., H. Le-Niculescu, D.F. Levey, N. Jain, B. Changala, S.D. Patel, E. Winiger, A. Breier, A. Shekhar, R. Amdur, et al. 2012. Convergent functional genomics of schizophrenia: From comprehensive understanding to genetic risk prediction. *Mol. Psychiatry.* 17:887–905. https://doi.org/10.1038/mp.2012.37

Balendiran, G.K., F. Schnutgen, G. Scapin, T. Borchers, N. Xhong, K. Lim, R. Godbout, F. Spener, and J.C. Sacchettini. 2000. Crystal structure and thermodynamic analysis of human brain fatty acid-binding protein. *J. Biol. Chem.* 275:27045–27054. https://doi.org/10.1016/S0021-9258(19)61478-X

Battye, T.G.G., L. Kontogiannis, O. Johnson, H.R. Powell, and A.G.W. Leslie. 2011. iMOSFLM: A new graphical interface for diffraction-image processing with MOSFLM. *Acta Crystallogr. D Biol. Crystallogr.* 67:271–281. https://doi.org/10.1107/S0907444910048675

Brown, M.S., and J.L. Goldstein. 1986. A receptor-mediated pathway for cholesterol homeostasis (nobel lecture). *Angew. Chem. Int. Ed. Engl.* 25: 583–602. https://doi.org/10.1002/anie.198605833

Charman, M., B.E. Kennedy, N. Osborne, and B. Karten. 2010. MLN64 mediates egress of cholesterol from endosomes to mitochondria in the absence of functional Niemann-Pick Type C1 protein. *J. Lipid Res.* 51: 1023–1034. https://doi.org/10.1194/jlr.M002345

Chu, B.B., Y.C. Liao, W. Qi, C. Xie, X. Du, J. Wang, H. Yang, H.H. Miao, B.L. Li, and B.L. Song. 2015. Cholesterol transport through lysosome-peroxisome membrane contacts. *Cell.* 161:291–306. https://doi.org/10.1016/j.cell.2015.02.019

Das, A., M.S. Brown, D.D. Anderson, J.L. Goldstein, and A. Radhakrishnan. 2014. Three pools of plasma membrane cholesterol and their relation to cholesterol homeostasis. *eLife.* 3:e02882. https://doi.org/10.7554/eLife.02882

Dietschy, J.M. 2009. Central nervous system: Cholesterol turnover, brain development and neurodegeneration. *Biol. Chem.* 390:287–293. https://doi.org/10.1515/BC.2009.035

Dittman, J.S., and A.K. Menon. 2017. Speed limits for nonvesicular intracellular sterol transport. *Trends Biochem. Sci.* 42:90–97. https://doi.org/10.1016/j.tibs.2016.11.004

Dong, J., X. Du, H. Wang, J. Wang, C. Lu, X. Chen, Z. Zhu, Z. Luo, L. Yu, A.J. Brown, et al. 2019. Allosteric enhancement of ORP1-mediated cholesterol transport by PI(4,5)P_2/PI(3,4)P_2. *Nat. Commun.* 10:829. https://doi.org/10.1038/s41467-019-08791-0

Driessen, T.M., C. Zhao, M. Saenz, S.A. Stevenson, Y. Owada, and S.C. Gammie. 2018. Down-regulation of fatty acid binding protein 7 (Fabp7) is a hallmark of the postpartum brain. *J. Chem. Neuroanat.* 92:92–101. https://doi.org/10.1016/j.jchemneu.2018.07.003

Du, X., J. Kumar, C. Ferguson, T.A. Schulz, Y.S. Ong, W. Hong, W.A. Prinz, R.G. Parton, A.J. Brown, and H. Yang. 2011. A role for oxysterol-binding protein-related protein 5 in endosomal cholesterol trafficking. *J. Cell Biol.* 192:121–135. https://doi.org/10.1083/jcb.201004142

Ebrahimi, M., Y. Yamamoto, K. Sharifi, H. Kida, Y. Kagawa, Y. Yasumoto, A. Islam, H. Miyazaki, C. Shimamoto, M. Maekawa, et al. 2016. Astrocyte-expressed FABP7 regulates dendritic morphology and excitatory synaptic function of cortical neurons. *Glia.* 64:48–62. https://doi.org/10.1002/glia.22902

Elsherbiny, M.E., M. Emara, and R. Godbout. 2013. Interaction of brain fatty acid-binding protein with the polyunsaturated fatty acid environment as a potential determinant of poor prognosis in malignant glioma. *Prog. Lipid Res.* 52:562–570. https://doi.org/10.1016/j.plipres.2013.08.004

Emsley, P., and K. Cowtan. 2004. Coot: Model-building tools for molecular graphics. *Acta Crystallogr. D Biol. Crystallogr.* 60:2126–2132. https://doi.org/10.1107/S0907444904019158

Fujita, M., H. Fujii, T. Kanda, E. Sato, K. Hatakeyama, and T. Ono. 1995. Molecular cloning, expression, and characterization of a human intestinal 15-kDa protein. *Eur. J. Biochem.* 233:406–413. https://doi.org/10.1111/j.1432-1033.1995.406_2.x

Gong, Y.Z., E.T. Everett, D.A. Schwartz, J.S. Norris, and F.A. Wilson. 1994. Molecular cloning, tissue distribution, and expression of a 14-kDa bile acid-binding protein from rat ileal cytosol. *Proc. Natl. Acad. Sci. USA.* 91: 4741–4745. https://doi.org/10.1073/pnas.91.11.4741

Haunerland, N.H., and F. Spener. 2004. Fatty acid-binding proteins--insights from genetic manipulations. *Prog. Lipid Res.* 43:328–349. https://doi.org/10.1016/j.plipres.2004.05.001

Heybrock, S., K. Kanerva, Y. Meng, C. Ing, A. Liang, Z.J. Xiong, X. Weng, Y. Ah Kim, R. Collins, W. Trimble, et al. 2019. Lysosomal integral membrane protein-2 (LIMP-2/SCARB2) is involved in lysosomal cholesterol export. *Nat. Commun.* 10:3521. https://doi.org/10.1038/s41467-019-11425-0

Höglinger, D., T. Burgoyne, E. Sanchez-Heras, P. Hartwig, A. Colaco, J. Newton, C.E. Futter, S. Spiegel, F.M. Platt, and E.R. Eden. 2019. NPC1 regulates ER contacts with endocytic organelles to mediate cholesterol egress. *Nat. Commun.* 10:4276. https://doi.org/10.1038/s41467-019-12152-2

Hu, A., J.Z. Zhang, J. Wang, C.C. Li, M. Yuan, G. Deng, Z.C. Lin, Z.P. Qiu, H.Y. Liu, X.W. Wang, et al. 2022. Cholesterylation of Smoothened is a calcium-accelerated autoreaction involving an intramolecular ester intermediate. *Cell Res.* 32:288–301. https://doi.org/10.1038/s41422-022-00622-0

Infante, R.E., and A. Radhakrishnan. 2017. Continuous transport of a small fraction of plasma membrane cholesterol to endoplasmic reticulum regulates total cellular cholesterol. *Elife.* 6:e25466. https://doi.org/10.7554/eLife.25466

Ishitsuka, R., T. Saito, H. Osada, Y. Ohno-Iwashita, and T. Kobayashi. 2011. Fluorescence image screening for chemical compounds modifying cholesterol metabolism and distribution. *J. Lipid Res.* 52:2084–2094. https://doi.org/10.1194/jlr.D018184

Iwayama, Y., E. Hattori, M. Maekawa, K. Yamada, T. Toyota, T. Ohnishi, Y. Iwata, K.J. Tsuchiya, G. Sugihara, M. Kikuchi, et al. 2010. Association analyses between brain-expressed fatty-acid binding protein (FABP) genes and schizophrenia and bipolar disorder. *Am. J. Med. Genet. B. Neuropsychiatr. Genet.* 153B:484–493. https://doi.org/10.1002/ajmg.b.31004

Jensen, K.G., C.U. Correll, D. Rudå, D.G. Klauber, M. Stentebjerg-Olesen, B. Fagerlund, J.R.M. Jepsen, A. Fink-Jensen, and A.K. Pagsberg. 2017. Pretreatment cardiometabolic status in youth with early-onset psychosis: Baseline results from the TEA trial. *J. Clin. Psychiatry.* 78: e1035–e1046. https://doi.org/10.4088/JCP.15m10479

Kanerva, K., R.L. Uronen, T. Blom, S. Li, R. Bittman, P. Lappalainen, J. Peränen, G. Raposo, and E. Ikonen. 2013. LDL cholesterol recycles to the plasma membrane via a Rab8a-Myosin5b-actin-dependent membrane transport route. *Dev. Cell*. 27:249–262. https://doi.org/10.1016/j.devcel.2013.09.016

Khan, R., J.E. Lee, Y.M. Yang, F.X. Liang, and P.B. Sehgal. 2013. Live-cell imaging of the association of STAT6-GFP with mitochondria. *PLoS One*. 8:e55426. https://doi.org/10.1371/journal.pone.0055426

Kwon, H.J., L. Abi-Mosleh, M.L. Wang, J. Deisenhofer, J.L. Goldstein, M.S. Brown, and R.E. Infante. 2009. Structure of N-terminal domain of NPC1 reveals distinct subdomains for binding and transfer of cholesterol. *Cell*. 137:1213–1224. https://doi.org/10.1016/j.cell.2009.03.049

Li, J., and S.R. Pfeffer. 2016. Lysosomal membrane glycoproteins bind cholesterol and contribute to lysosomal cholesterol export. *Elife*. 5:e21635. https://doi.org/10.7554/eLife.21635

Liu, R.Z., R. Mita, M. Beaulieu, Z. Gao, and R. Godbout. 2010. Fatty acid binding proteins in brain development and disease. *Int. J. Dev. Biol.* 54: 1229–1239. https://doi.org/10.1387/ijdb.092976rl

Luo, J., L. Jiang, H. Yang, and B.L. Song. 2017. Routes and mechanisms of post-endosomal cholesterol trafficking: A story that never ends. *Traffic*. 18: 209–217. https://doi.org/10.1111/tra.12471

Luo, J., L.Y. Jiang, H. Yang, and B.L. Song. 2019. Intracellular cholesterol transport by sterol transfer proteins at membrane contact sites. *Trends Biochem. Sci.* 44:273–292. https://doi.org/10.1016/j.tibs.2018.10.001

Maekawa, M., and G.D. Fairn. 2015. Complementary probes reveal that phosphatidylserine is required for the proper transbilayer distribution of cholesterol. *J. Cell Sci.* 128:1422–1433. https://doi.org/10.1242/jcs.164715

Majava, V., E. Polverini, A. Mazzini, R. Nanekar, W. Knoll, J. Peters, F. Natali, P. Baumgärtel, I. Kursula, and P. Kursula. 2010. Structural and functional characterization of human peripheral nervous system myelin protein P2. *PLoS One*. 5:e10300. https://doi.org/10.1371/journal.pone.0010300

Malnar, M., S. Hecimovic, N. Mattsson, and H. Zetterberg. 2014. Bidirectional links between Alzheimer's disease and Niemann-Pick type C disease. *Neurobiol. Dis.* 72:37–47. https://doi.org/10.1016/j.nbd.2014.05.033

Martin, G.G., B.P. Atshaves, H. Huang, A.L. McIntosh, B.J. Williams, P.J. Pai, D.H. Russell, A.B. Kier, and F. Schroeder. 2009. Hepatic phenotype of liver fatty acid binding protein gene-ablated mice. *Am. J. Physiol. Gastrointest. Liver Physiol.* 297:G1053–G1065. https://doi.org/10.1152/ajpgi.00116.2009

McCoy, A.J., R.W. Grosse-Kunstleve, P.D. Adams, M.D. Winn, L.C. Storoni, and R.J. Read. 2007. Phaser crystallographic software. *J. Appl. Cryst.* 40: 658–674. https://doi.org/10.1107/S0021889807021206

Mita, R., M.J. Beaulieu, C. Field, and R. Godbout. 2010. Brain fatty acid-binding protein and omega-3/omega-6 fatty acids: Mechanistic insight into malignant glioma cell migration. *J. Biol. Chem.* 285:37005–37015. https://doi.org/10.1074/jbc.M110.170076

Mollenhauer, B., P. Steinacker, E. Bahn, M. Bibl, P. Brechlin, M.G. Schlossmacher, J.J. Locascio, J. Wiltfang, H.A. Kretzschmar, S. Poser, et al. 2007. Serum heart-type fatty acid-binding protein and cerebrospinal fluid tau: Marker candidates for dementia with lewy bodies. *Neurodegener. Dis.* 4:366–375. https://doi.org/10.1159/000105157

Nemecz, G., and F. Schroeder. 1991. Selective binding of cholesterol by recombinant fatty acid binding proteins. *J. Biol. Chem.* 266:17180–17186. https://doi.org/10.1016/S0021-9258(19)47356-0

Nixon, R.A. 2004. Niemann-pick type C disease and Alzheimer's disease: The APP-endosome connection fattens up. *Am. J. Pathol.* 164:757–761. https://doi.org/10.1016/S0002-9440(10)63163-X

Pfisterer, S.G., J. Peränen, and E. Ikonen. 2016. LDL-Cholesterol transport to the endoplasmic reticulum: Current concepts. *Curr. Opin. Lipidol.* 27: 282–287. https://doi.org/10.1097/MOL.0000000000000292

Porter, J.A., K.E. Young, and P.A. Beachy. 1996. Cholesterol modification of hedgehog signaling proteins in animal development. *Science*. 274: 255–259. https://doi.org/10.1126/science.274.5285.255

Qiu, Z.P., Z.C. Lin, A. Hu, Y.B. Liu, W.E. Zeng, X. Zhao, X.J. Shi, J. Luo, and B.L. Song. 2023. GRAMD1/ASTER-mediated cholesterol transport promotes Smoothened cholesterylation at the endoplasmic reticulum. *EMBO J.* 42: e111513. https://doi.org/10.15252/embj.2022111513

Rademacher, M., A.W. Zimmerman, H. Rüterjans, J.H. Veerkamp, and C. Lücke. 2002. Solution structure of fatty acid-binding protein from human brain. *Mol. Cell. Biochem.* 239:61–68. https://doi.org/10.1023/A:1020566909213

Richieri, G.V., R.T. Ogata, and A.M. Kleinfeld. 1994. Equilibrium constants for the binding of fatty acids with fatty acid-binding proteins from adipocyte, intestine, heart, and liver measured with the fluorescent probe ADIFAB. *J. Biol. Chem.* 269:23918–23930. https://doi.org/10.1016/S0021-9258(19)51026-2

Sepe, F.N., D. Chiasserini, and L. Parnetti. 2018. Role of FABP3 as biomarker in Alzheimer's disease and synucleinopathies. *Future Neurol.* 13:199–207. https://doi.org/10.2217/fnl-2018-0003

Shimamoto, C., T. Ohnishi, M. Maekawa, A. Watanabe, H. Ohba, R. Arai, Y. Iwayama, Y. Hisano, T. Toyota, M. Toyoshima, et al. 2014. Functional characterization of FABP3, 5 and 7 gene variants identified in schizophrenia and autism spectrum disorder and mouse behavioral studies. *Hum. Mol. Genet.* 23:6495–6511. https://doi.org/10.1093/hmg/ddu369

Smathers, R.L., and D.R. Petersen. 2011. The human fatty acid-binding protein family: Evolutionary divergences and functions. *Hum. Genomics*. 5: 170–191. https://doi.org/10.1186/1479-7364-5-3-170

Storch, J., and B. Corsico. 2008. The emerging functions and mechanisms of mammalian fatty acid-binding proteins. *Annu. Rev. Nutr.* 28:73–95. https://doi.org/10.1146/annurev.nutr.27.061406.093710

Teunissen, C.E., R. Veerhuis, J. De Vente, F.R.J. Verhey, F. Vreeling, M.P.J. van Boxtel, J.F.C. Glatz, and M.A.L. Pelsers. 2011. Brain-specific fatty acid-binding protein is elevated in serum of patients with dementia-related diseases. *Eur. J. Neurol.* 18:865–871. https://doi.org/10.1111/j.1468-1331.2010.03273.x

Trinh, M.N., M.S. Brown, J.L. Goldstein, J. Han, G. Vale, J.G. McDonald, J. Seemann, J.T. Mendell, and F. Lu. 2020. Last step in the path of LDL cholesterol from lysosome to plasma membrane to ER is governed by phosphatidylserine. *Proc. Natl. Acad. Sci. USA*. 117:18521–18529. https://doi.org/10.1073/pnas.2010682117

Vanier, M.T. 2010. Niemann-Pick disease type C. *Orphanet J. Rare Dis.* 5:16. https://doi.org/10.1186/1750-1172-5-16

Wang, H., Q. Ma, Y. Qi, J. Dong, X. Du, J. Rae, J. Wang, W.F. Wu, A.J. Brown, R.G. Parton, et al. 2019. Orp2 delivers cholesterol to the plasma membrane in exchange for phosphatidylinositol 4, 5-bisphosphate (PI (4,5) P2). *Mol. Cell*. 73:458–473.e7. https://doi.org/10.1016/j.molcel.2018.11.014

Wang, J.Q., Z.C. Lin, L.L. Li, S.F. Zhang, W.H. Li, W. Liu, B.L. Song, and J. Luo. 2021. SUMOylation of the ubiquitin ligase IDOL decreases LDL receptor levels and is reversed by SENP1. *J. Biol. Chem.* 296:100032. https://doi.org/10.1074/jbc.RA120.015420

Wilhelm, L.P., C. Wendling, B. Védie, T. Kobayashi, M.P. Chenard, C. Tomasetto, G. Drin, and F. Alpy. 2017. STARD3 mediates endoplasmic reticulum-to-endosome cholesterol transport at membrane contact sites. *EMBO J.* 36:1412–1433. https://doi.org/10.15252/embj.201695917

Winkler, M.B.L., R.T. Kidmose, M. Szomek, K. Thaysen, S. Rawson, S.P. Muench, D. Wüstner, and B.P. Pedersen. 2019. Structural insight into eukaryotic sterol transport through niemann-pick type C proteins. *Cell*. 179:485–497.e18. https://doi.org/10.1016/j.cell.2019.08.038

Winn, M.D., C.C. Ballard, K.D. Cowtan, E.J. Dodson, P. Emsley, P.R. Evans, R.M. Keegan, E.B. Krissinel, A.G.W. Leslie, A. McCoy, et al. 2011. Overview of the CCP4 suite and current developments. *Acta Crystallogr. D Biol. Crystallogr.* 67:235–242. https://doi.org/10.1107/S0907444910045749

Wolfrum, C. 2007. Cytoplasmic fatty acid binding protein sensing fatty acids for peroxisome proliferator activated receptor activation. *Cell. Mol. Life Sci.* 64:2465–2476. https://doi.org/10.1007/s00018-007-7279-4

Wolozin, B. 2004. Cholesterol and the biology of Alzheimer's disease. *Neuron*. 41:7–10. https://doi.org/10.1016/S0896-6273(03)00840-7

Wong, L.H., A.T. Gatta, and T.P. Levine. 2019. Lipid transfer proteins: The lipid commute via shuttles, bridges and tubes. *Nat. Rev. Mol. Cell Biol.* 20:85–101. https://doi.org/10.1038/s41580-018-0071-5

Woods, A.G., I. Sokolowska, R. Taurines, M. Gerlach, E. Dudley, J. Thome, and C.C. Darie. 2012. Potential biomarkers in psychiatry: Focus on the cholesterol system. *J. Cell. Mol. Med.* 16:1184–1195. https://doi.org/10.1111/j.1582-4934.2012.01543.x

Xiao, J., J. Luo, A. Hu, T. Xiao, M.X. Li, Z.K. Kong, L.Y. Jiang, Z.M. Zhou, Y.C. Liao, C. Xie, et al. 2019. Cholesterol transport through the peroxisome-ER membrane contacts tethered by PI(4,5)P_2 and extended synaptotagmins. *Sci. China Life Sci.* 62:1117–1135. https://doi.org/10.1007/s11427-019-9569-9

Xiao, J., B.L. Song, and J. Luo. 2021a. Peroxisomes in intracellular cholesterol transport: From basic physiology to brain pathology. *Explor. Neuroprotective Ther.* 1:127–145. https://doi.org/10.37349/ent.2021.00011

Xiao, J., Y. Xiong, L.T. Yang, J.Q. Wang, Z.M. Zhou, L.W. Dong, X.J. Shi, X. Zhao, J. Luo, and B.L. Song. 2021b. POST1/C12ORF49 regulates the SREBP pathway by promoting site-1 protease maturation. *Protein Cell*. 12:279–296. https://doi.org/10.1007/s13238-020-00753-3

Xiao, X., J.J. Tang, C. Peng, Y. Wang, L. Fu, Z.P. Qiu, Y. Xiong, L.F. Yang, H.W. Cui, X.L. He, et al. 2017. Cholesterol modification of smoothened is required for hedgehog signaling. *Mol. Cell*. 66:154–162.e10. https://doi.org/10.1016/j.molcel.2017.02.015

Zhao, K., and N.D. Ridgway. 2017. Oxysterol-binding protein-related protein 1l regulates cholesterol egress from the endo-lysosomal system. *Cell Rep.* 19:1807–1818. https://doi.org/10.1016/j.celrep.2017.05.028

Zhao, K., J. Foster, and N.D. Ridgway. 2020. Oxysterol-binding protein-related protein 1 variants have opposing cholesterol transport activities from the endolysosomes. *Mol. Biol. Cell.* 31:793–802. https://doi.org/10.1091/mbc.E19-12-0697

Zhou, Y.X., J. Wei, G. Deng, A. Hu, P.Y. Sun, X. Zhao, B.L. Song, and J. Luo. 2023. Delivery of low-density lipoprotein from endocytic carriers to mitochondria supports steroidogenesis. *Nat. Cell Biol.* 25:937–949. https://doi.org/10.1038/s41556-023-01160-6

Ziats, M.N., and O.M. Rennert. 2011. Expression profiling of autism candidate genes during human brain development implicates central immune signaling pathways. *PLoS One.* 6:e24691. https://doi.org/10.1371/journal.pone.0024691

JCB

Supplemental material

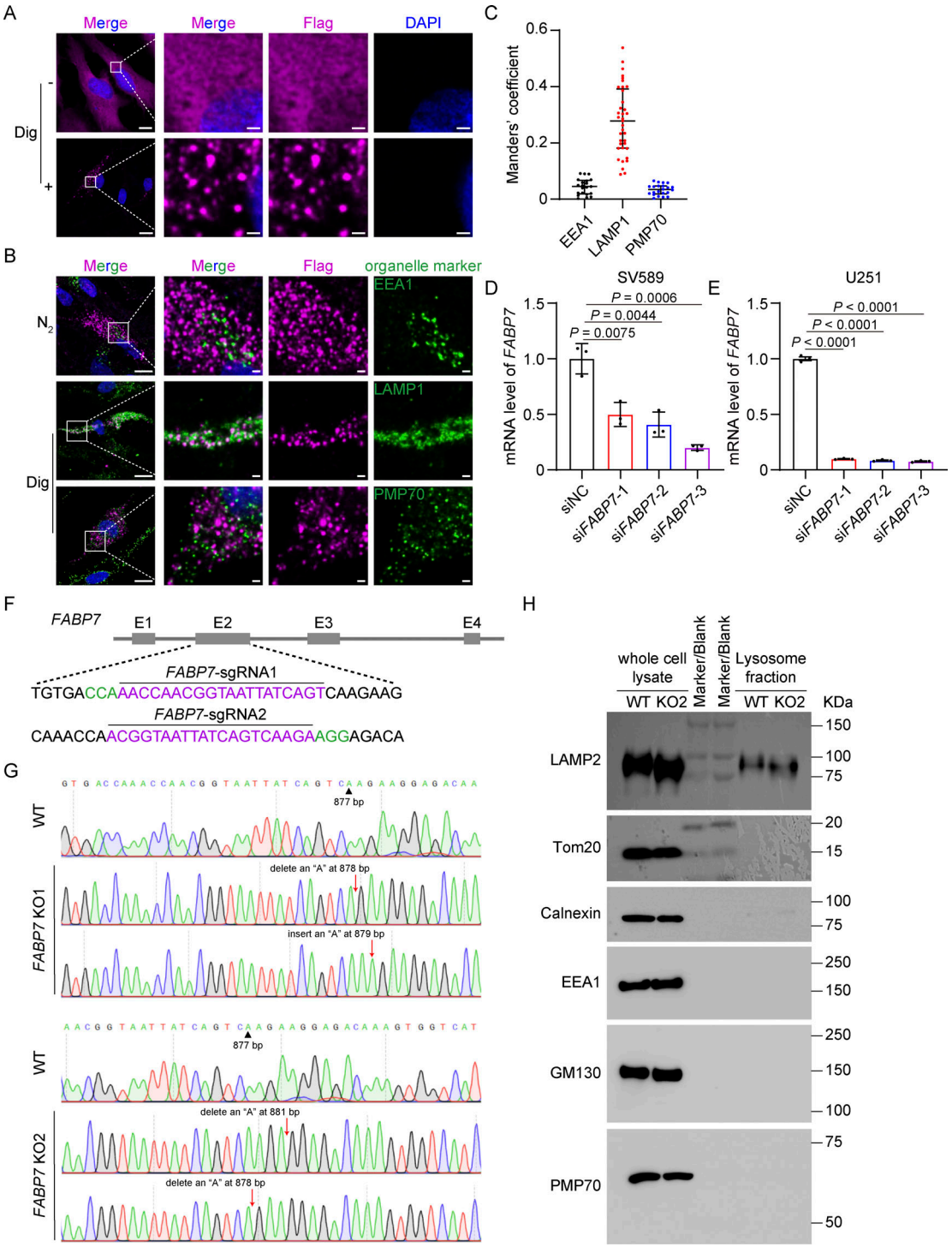

Figure S1. **The subcellular localization of FABP7 and characterization of *FABP7* knockdown and knockout in cultured cells. (A)** SV589 cells infected with lentivirus expressing FABP7-Flag were permeabilized without (–) or with (+) 0.005% digitonin (Dig) diluted in DMEM containing 0.3 M sucrose for 5 min before fixation with 4% PFA for 30 min at room temperature. Boxed areas are shown at a higher magnification on the right. Scale bars, 10 µm (main), 1 µm (inset). **(B)** Cells were permeabilized in a liquid nitrogen bath (N_2) for 30 s before fixation and immunostained with anti-Flag and anti-EEA1 antibodies, or permeabilized with digitonin (Dig) as described above and immunostained with anti-Flag antibody and other organelle markers. Boxed areas are shown at a higher magnification on the right. Scale bars, 10 µm (main), 1 µm (inset). **(C)** Quantification of FABP7 colocalization with organelle-specific markers. Data are presented as mean ± SEM (n = 80 cells from three independent experiments). **(D and E)** Knockdown efficiency of *FABP7* in SV589 fibroblasts (D) and U251 cells (E). Indicated cells were transfected with the indicated siRNAs for 48 h and harvested for quantitative PCR (qPCR). The mRNA abundance of indicated cells transfected with scrambled control siRNA (NC, negative control) is defined as 1 and used as the reference for comparison. Data are presented as mean ± SEM (from three biological replicates). **(F)** Cartoon showing that the exon (E) 2 of the human *FABP7* gene was edited by Cas9/sgRNA. Two targeting sequences are in magenta and the protospacer-adjacent motifs are in green. **(G)** Sanger sequencing of two lines of *FABP7* KO cells. **(H)** WT and *FABP7* KO2 cells were harvested, and lysosomes were purified and subjected to immunoblotting analysis. Related to Fig. 1 G. Source data are available for this figure: SourceData FS1.

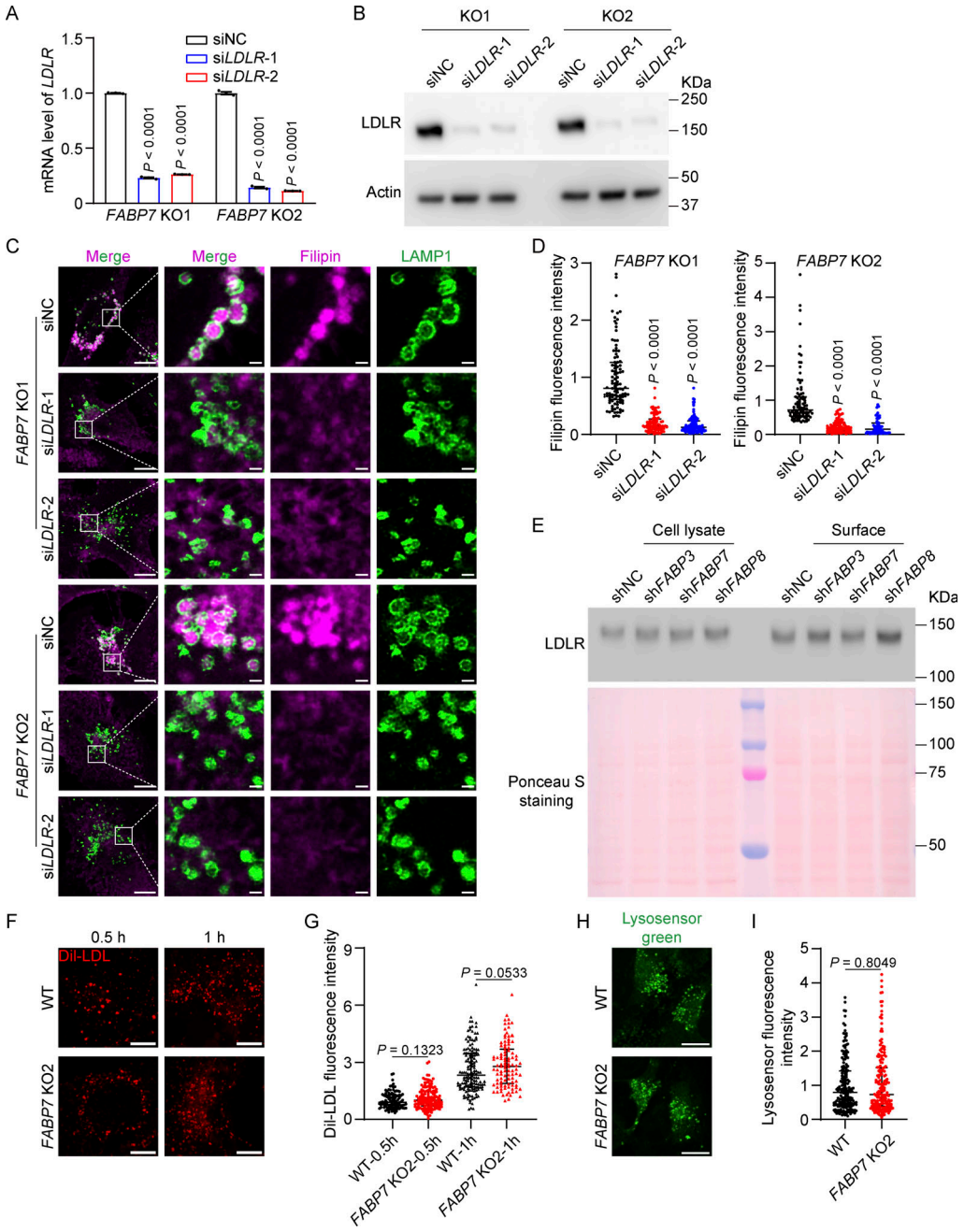

Figure S2. **LDLR-mediated LDL uptake provides cholesterol for FABP7-mediated transport. (A and B)** Two lines of *FABP7* KO cells (*FABP7* KO1 and *FABP7* KO2) were transfected with the indicated siRNAs for 48 h and harvested for qPCR (A) and immunoblotting (B) to determine the knockdown efficiency of *LDLR* gene and the resultant reduction in LDLR protein, respectively. The mRNA abundance of indicated cells transfected with scrambled control siRNA (NC, negative control) is defined as 1 and used as the reference for comparison. Data are presented as mean ± SEM (from three biological replicates). **(C and D)** Two lines of *FABP7* KO cells (*FABP7* KO1 and *FABP7* KO2) were transfected with the indicated siRNAs for 48 h transfection, fixed, and stained with filipin (magenta) and the anti-LAMP1 antibody (green). Boxed areas are shown at a higher magnification on the right. Scale bars, 10 µm (main), 1 µm (inset). NC, negative control. Relative fluorescence intensity of filipin in C was quantified by ImageJ and shown in D. The filipin fluorescence intensity of indicated cells transfected with scrambled control siRNA (NC, negative control) is defined as 1 and used as the reference for comparison. Data are presented as median with interquartile range (n = 575 cells from three independent experiments). Mann–Whitney U test. **(E)** SV589 fibroblasts were infected with lentivirus expressing indicated shRNAs and harvested for surface biotinylation assay. Ponceau S staining indicates equal amounts of samples were loaded. **(F)** WT and *FABP7* KO2 cells were washed with PBS and incubated in lipoprotein-deficient medium (5% lipoprotein-deficient serum) supplemented with 10 µg/ml Dil-labeled LDL for the indicated time point. Scale bars, 10 µm. **(G)** Quantification of relative fluorescence intensity of the internalized Dil-LDL in F. The Dil-LDL fluorescence intensity of wild-type (WT) cells incubated with LDL for 0.5 h is defined as 1 and used as the reference for comparison. Data are presented as median with interquartile range (n = 497 cells from three independent experiments). Mann–Whitney U test. **(H)** WT and *FABP7* KO2 cells were subjected to LysoSensor Green staining to assess lysosomal acidity. Scale bars, 10 µm. **(I)** Quantification of LysoSensor fluorescence intensity in H. The LysoSensor fluorescence intensity of wild-type (WT) cells is defined as 1 and used as the reference for comparison. Data are presented as median with interquartile range (n = 366 cells from three independent experiments). Mann–Whitney U test. Source data are available for this figure: SourceData FS2.

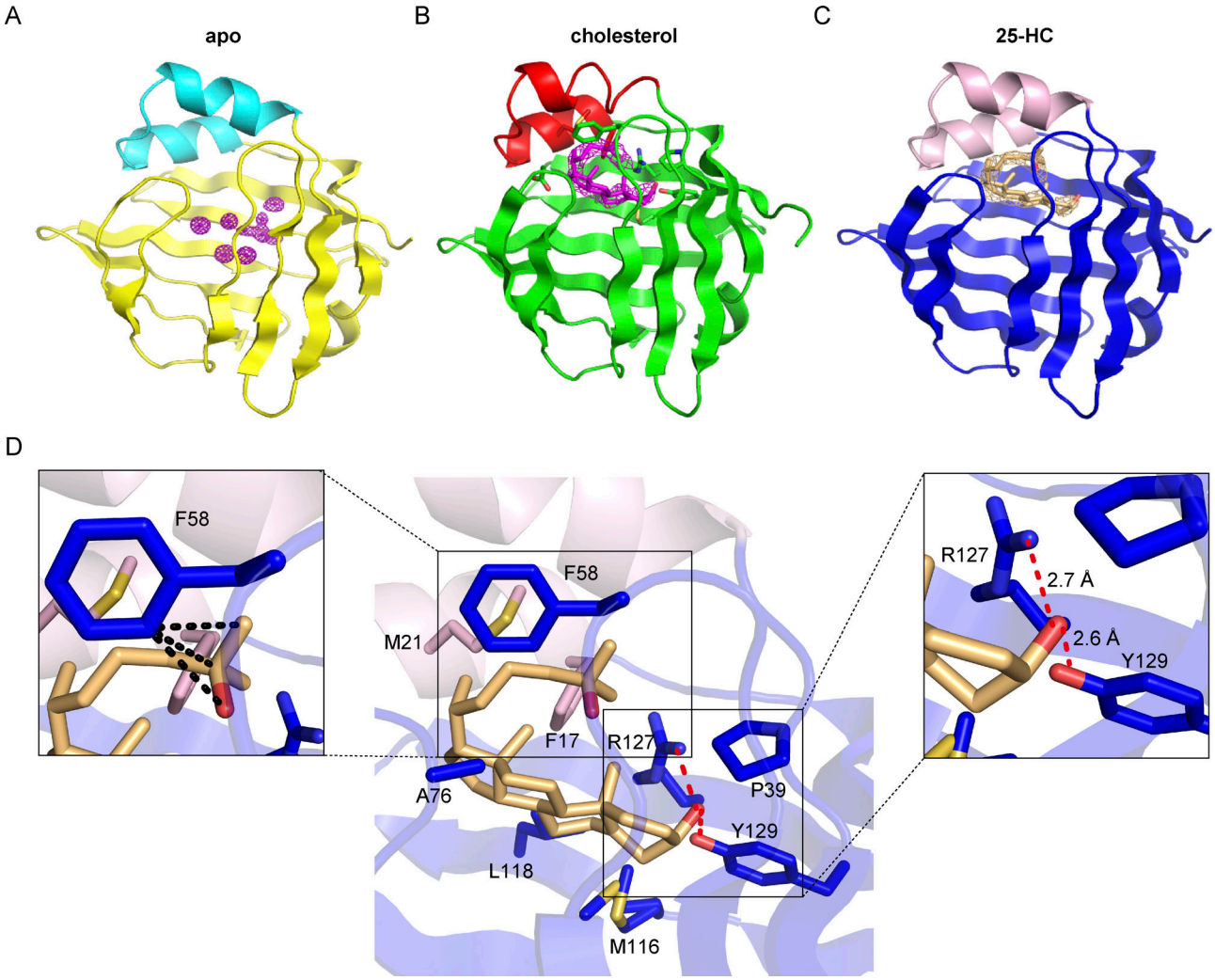

Figure S3. **Crystal structure of apo and ligand-binding FABP7. (A–C)** The *2Fo-Fc* electron density map showing FABP7 with water and cholesterol and 25-HC as the ligand. **(D)** Detailed view of FABP7 interacting with 25-HC (light orange sticks). Hydrogen bonds formed between FABP7 and the hydroxyl group of 25-HC are denoted by red dashed lines. The hydrophobic interactions between FABP7 F58 and 25-HC are shown by black dashed lines. Key residues for 25-HC binding are indicated.

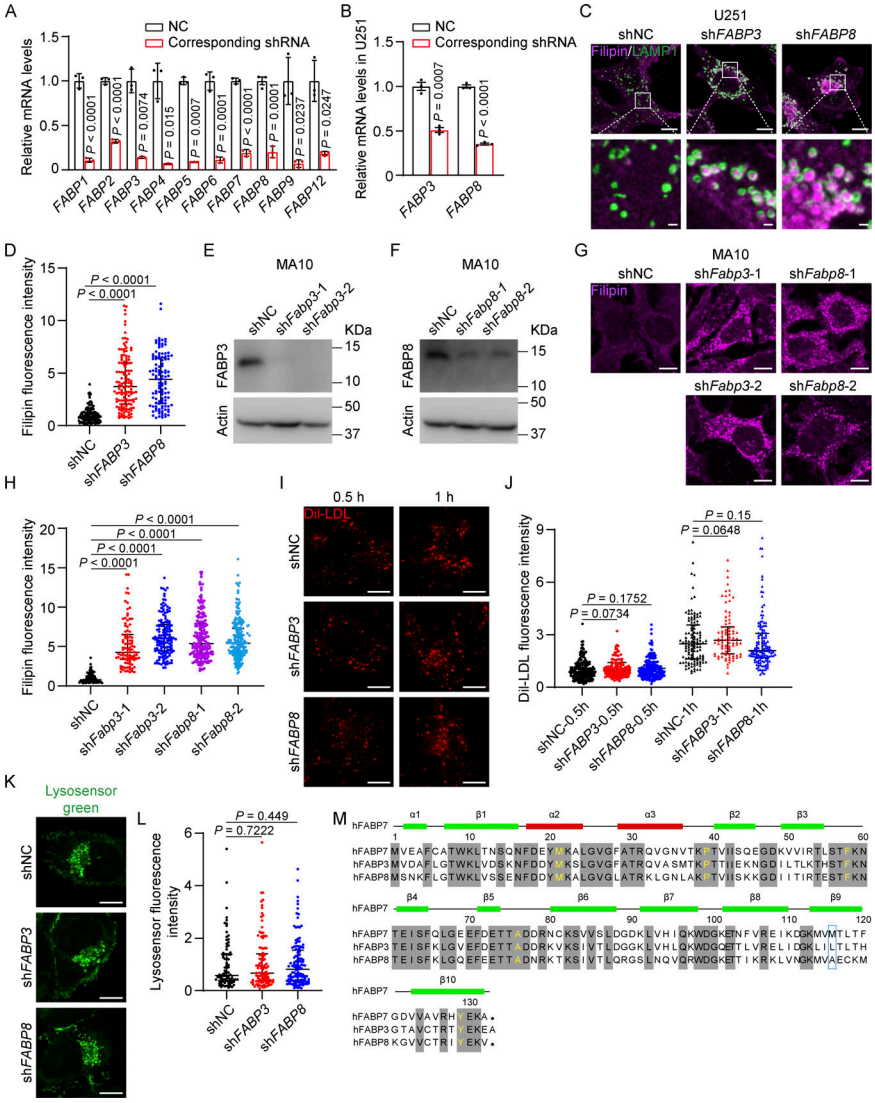

Figure S4. **Cholesterol accumulation in the cells lacking FABP3 or FABP8. (A)** Knockdown efficiency of human *FABP7* family members determined by qPCR. Related to Fig. 7 A. The mRNA abundance of indicated cells infected with lentivirus expressing scrambled control shRNA (NC, negative control) is defined as 1 and used as the reference for comparison. Data are presented as mean ± SEM (from three biological replicates). **(B–D)** U251 cells were infected with lentivirus expressing the indicated shRNAs and harvested. **(B)** Knockdown efficiency of *FABP3* and *FABP8* determined by qPCR. The mRNA abundance of indicated cells infected with lentivirus expressing scrambled control shRNA (NC, negative control) is defined as 1 and used as the reference for comparison. Data are presented as mean ± SEM analysis (from three biological replicates). **(C)** U251 cells were fixed and stained with filipin (magenta) and the anti-LAMP1 antibody (green). Boxed areas are shown at a higher magnification on the bottom. Scale bars, 10 µm (main), 1 µm (inset). **(D)** Quantification of relative fluorescence intensity of filipin in C. The filipin fluorescence intensity of cells infected with lentivirus expressing scrambled control shRNA (NC, negative control) is defined as 1 and used as the reference for comparison. Data are presented as median with interquartile range (n = 361 cells from three independent experiments). Mann–Whitney U test. **(E–H)** MA10 cells were infected with lentivirus expressing the indicated shRNAs and harvested. NC, negative control. **(E and F)** Immunoblotting analysis showing *Fabp3* or *Fabp8* knockdown MA10 cells. **(G)** MA10 cells were fixed and stained with filipin (magenta). Scale bars, 10 µm. **(H)** Quantification of relative fluorescence intensity of filipin in G. The filipin fluorescence intensity of cells infected with lentivirus expressing scrambled control shRNA (NC, negative control) is defined as 1 and used as the reference for comparison. Data are presented as median with interquartile range (n = 749 cells from three independent experiments). Mann–Whitney U test. **(I)** SV589 cells were infected with lentivirus expressing the indicated shRNAs, washed with PBS and incubated in lipoprotein-deficient medium (5% lipoprotein-deficient serum) supplemented with 10 µg/ml Dil-labeled LDL for indicated time point. NC, negative control. Scale bars, 10 µm. **(J)** Quantification of relative fluorescence intensity of the internalized Dil-LDL in I. The Dil-LDL fluorescence intensity of cells infected with lentivirus expressing scrambled control shRNA (NC, negative control) and incubated with LDL for 0.5 h is defined as 1 and used as the reference for comparison. Data are presented as median with interquartile range (n = 828 cells from three independent experiments). Mann–Whitney U test. **(K)** SV589 cells were infected with lentivirus expressing the indicated shRNAs, and subjected to LysoSensor Green staining. NC, negative control. **(L)** Quantification of LysoSensor fluorescence intensity in K. The LysoSensor fluorescence intensity of cells infected with lentivirus expressing scrambled control shRNA (NC, negative control) is defined as 1 and used as the reference for comparison. Data are presented as median with interquartile range (n = 413 cells from three independent experiments). Mann–Whitney U test. ns, no significance. **(M)** Sequence alignments of FABP7, 3, and 8. The residues conserved in all three FABPs are in shadow. The residues critical for cholesterol binding and transport are in yellow. The residues involved in cholesterol binding and transport but not conserved are circled in the blue box. h, human. Source data are available for this figure: SourceData FS4.

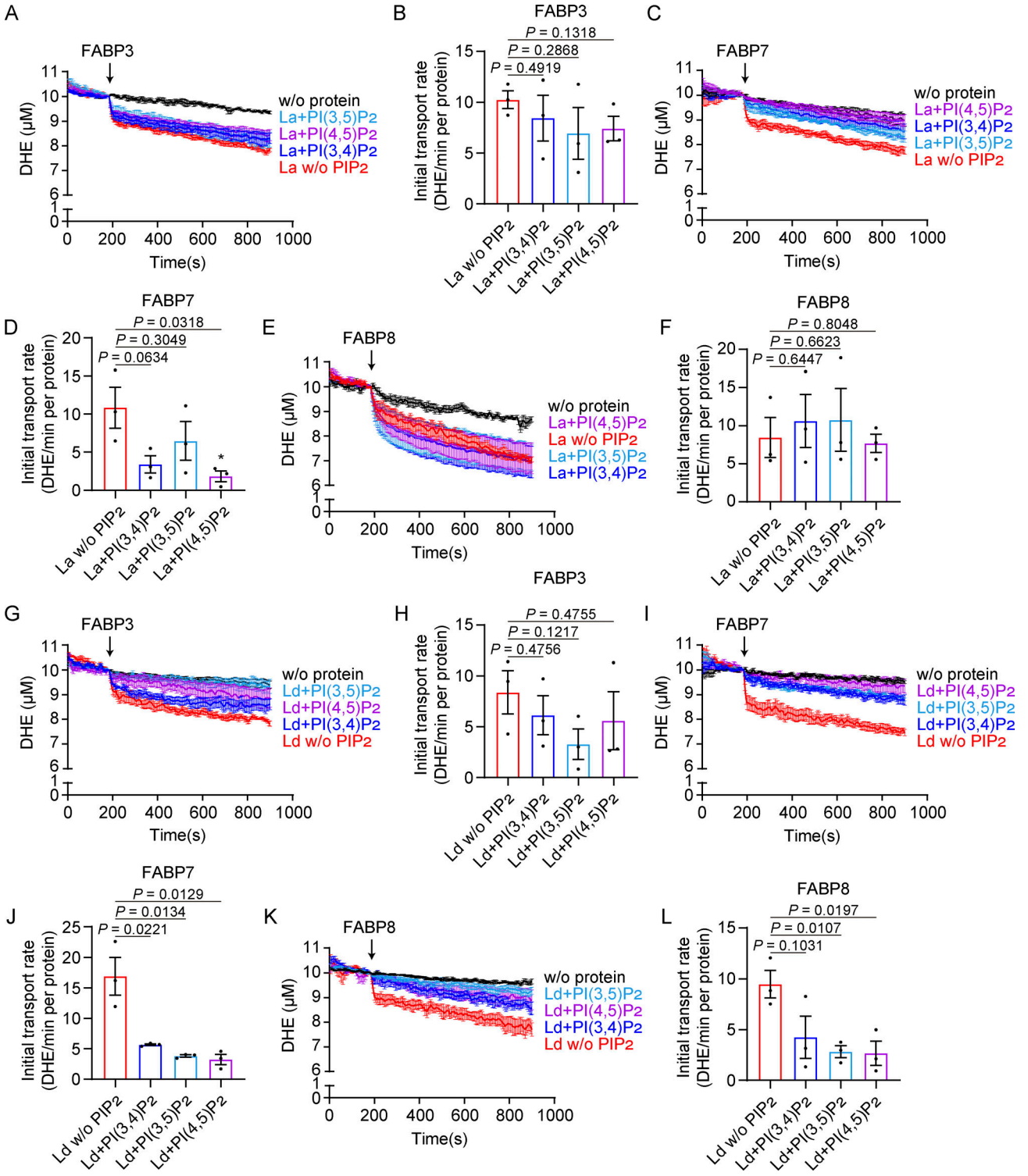

Figure S5. **PIP_2 does not enhance DHE transport by FABPs. (A–F)** The effects of PIP_2 species in the acceptor liposome (La) on DHE transport by FABP3 (A and B), FABP7 (C and D), or FABP8 (E and F). Arrow indicates when proteins were added. Initial transport rates were quantified in B, D, and F. Data are presented as mean ± SEM (from three independent experiments). Student's unpaired two-tailed *t* test. Compared with initial transport rates of DHE by indicated FABP proteins using the acceptor liposome without PIP_2. **(G–L)** The effects of PIP_2 species in the donor liposome (Ld) on DHE transport by FABP3 (G and H), FABP7 (I and J), or FABP8 (K and L). Arrow indicates when proteins were added. Initial transport rates were quantified in H, J, and L. Data are presented as mean ± SEM (from three independent experiments). Student's unpaired two-tailed *t* test. Compared with initial transport rates of DHE by indicated FABP proteins using the donor liposome without PIP_2.

Provided online are Table S1 and Table S2. Table S1 shows data collection and refinement statistics. Table S2 shows the full sequences of oligos used in this study.